Mixed Perovskites (2D/3D) based Solar Cells: A Review on crystallization and surface modification for enhanced efficiency and stability

Xiaohui Li[a], *Putao Zhang*[a,*], *Shengjun Li* [a,*], *Priyanka Wasnik,*[b,c] *Junna Ren,*[c,d] *Qinglong Jiang,*[b] *Ben Bin Xu,*[c] *and Vignesh Murugadoss*[d,*]

[a]Key Laboratory of Photovoltaic Materials, Henan University, Kaifeng, Henan, 475004, China.
[b]Department of Chemistry and Physics, University of Arkansas, Pine Bluff, AR, 71601, USA
[c]Mechanical and Construction Engineering, Faculty of Engineering and Environment, Northumbria University, Newcastle Upon Tyne, NE1 8ST, UK
[d]College of Materials Science and Engineering, Taiyuan University of Science and Technology, Taiyuan, 030024, China
[d]Membrane and Separation Technology Division, CSIR - Central Glass and Ceramic Research Institute, 196 Raja S.C. Mullick Road, Jadavpur University PO, Kolkata 700 032.

E-mail: putaozhang@henu.edu.cn; lishengjun@henu.edu.cn; vigneshmurugadoss15@gmail.com

Abstract

Solar cells based on a three-dimensional (3D) crystalline perovskite framework exhibit desired photoconversion efficiency. However, 3D perovskites are prone to surface defects, leading to severe Shockley-Read-Hall (SRH) recombination and insufficient interactions between components, resulting in lower efficiency and stability. In contrast, two-dimensional (2D) perovskites have comparatively better excellent stability in hot and humid environments but suffer from lower efficiency. Recently, researchers reported that surface passivation of 3D perovskite by 2D perovskite improves the stability of solar cells without compromising their efficiency. In this review, the recent advances in surface modification of three-dimensional perovskites using two-dimensional perovskites are discussed. The crystal structures, photoelectric properties, and surface passivation strategies of 2D/3D perovskite solar cells with different components are systematically presented. Finally, the prospect of using two-dimensional perovskite passivation technology to further improve photovoltaic performance is discussed.

1. Introduction

In just thirteen years, the power conversion efficiency (PCE) of Organic-inorganic hybrid perovskite-based solar cells (PSCs) exceeded 25% from 3.8% [1] (the current certified efficiency is 25.7% [2]), which is comparable to that of commercial silicon solar cells (certified 26.7%). Organic-inorganic hybrid perovskites are ideal light-absorbing materials due to their adjustable band gap, large absorption coefficient, long carrier diffusion length, simple fabrication process, and low fabrication cost, thus having great application prospects [3-10]. Due to the fascinating properties and higher power efficiency, efforts towards the further improvement of the photovoltaic performance and stability of perovskite-based solar cells involve three stages, i.e. the growth of high quality perovskite films, the charge transport regulation, and passivation of defects [11, 12].

To promote the commercial development of perovskite photovoltaics, the coexistence of high efficiency and stability is a common goal pursued by researchers in photovoltaic devices. The most widely studied perovskites for solar cells are 3D halide perovskites of the general chemical formula ABX_3, where A can be Cs^+, $CH_3NH_3^+$ (MA^+), or $HC(NH_2)_2^+$ (FA), B can be Ge^{2+}, Sn^{2+}, or Pb^{2+}, and X can be Cl^-, Br^-, or I^-. This 3D framework with $[PbX_6]^{4-}$octahedra sharing six corners creates a favorable electronic structure with wide conduction and valence bands, which facilitates charge transport [13]. For 3D perovskite solar cells, poor stability is the main limitation that hinders commercialization [14]. Since the high hydrophilicity of perovskite can lead materials to absorb water from the surrounding environment and thereby induce the

formation of hydrate products, perovskite is inherently sensitive to water and oxygen and susceptible to intrusion, which hinders the long-term operational stability of perovskite photovoltaic cells. For this reason, researchers have invested a lot of work in further improving photovoltaic stability by adopting various approaches such as surface passivation, bulk doping, process engineering, and device structure optimization. In 2014, Seok et al. [15] first reported that the use of toluene as an antisolvent enabled the fabrication of solar cells with a significant 16.2% increase in PCE with negligible hysteresis. Since then, the use of antisolvent treatment has greatly been adopted in facilitating PSCs. On the other hand, precursor ligand molecular interactions in a solution related to the nature of the intermediate phase in subsequent cell development including counter solvents such as toluene [16], chlorobenzene (CB) [17-19], trifluorotoluene [20], diethyl ether [21], isopropyl alcohol (IPA) [22], methyl acetate (MeOAc) [23, 24], ethyl acetate (EA) [25, 26], triethyl phosphate (TEP) [27], etc. In 2020, Wang et al. [28] demonstrated that the surface carrier transport of methylammonium lead iodide ($MAPbI_3$) improved by the surface functionalization of phenethylammonium (PEA) ligands using single-crystal microplate samples. These multifaceted microporous plates with lateral size greater than 10 μm and thicknesses lesser than 1 μm are ideal model systems for physical studies of solar cell devices. The reduction in surface defect density of one order magnitude was observed after PEA functionalization reduced and this significantly suppressed carrier scattering. This is similar to the results obtained by Seite et al. [29] The addition of PEA ligands improved device performance, on the one hand may be

that for band transport in semiconductors, the diffusion constant is given by $D = \tau_s \kappa T/m$, the diffusivity near the surface region of the untreated microplate is reduced, scattering is more frequent and τ_s is shorter. Another is that the PEA ligand increases the structural rigidity of the perovskite lattice and the PEA functional group also eliminates the shallow energy trap states. Chen et al. [30] used two N-type organic dopants ("DMBI-2-Th and DMBI-2-Th-I") to control the electronic state of the bulk perovskite and elucidated the doping mechanism of perovskite and the correlation between electronic state and molecular structure. DMBI-2-Th-I and iodide ions with the DMBI group provide a faster electron transfer for the perovskite film, resulting in a more pronounced N-type doping effect. This significantly improves the electron state of $MAPbI_3$, including electron trap density, electron concentration, bipolar charge transport characteristics, and electron extraction efficiency, resulting in efficient p-i-n perovskite with an optimal PCE of 20.90% and a maximum V_{OC} of 1.13 V. As a result, the efficiency of perovskite solar cells gradually increased. However, due to the structural characteristics of 3D perovskite, it has an inherent sensitivity to water and oxygen which hinders the long-term operational stability of perovskite photovoltaic cells [31]. But still the stability problem has not been completely addressed. Stacking 2D perovskites on 3D perovskites is a promising interface treatment. Therefore, 2D/3D perovskite solar cells have been proposed and studied. Perovskites are classified into Ruddlesden-Popper (RP) phase, Dion-Jacobson (DJ) phase, alternating interlayer space cation (ACI) phase, and mixed organic ligand phase according to the type of splicing between organic spacer cations and inorganic

flat plates [32, 33]. Different properties of organic ligands play a role in the photovoltaic performance of 2D perovskite solar cells, such as chain length, conjugation, solubility, etc. Especially the diversity of the properties of organic spacer layers has a non-negligible influence on the properties of the corresponding perovskite crystals, which can make the corresponding perovskite thin films with different photovoltaic properties. It also helps to improve environmental stability. A more detailed explanation are given in later section that briefly introduce the 2D perovskites. However, the PCE of 2D PSCs still lags than that of the polycationic 3D PSCs due to their strongly bound excitons . In addition, the introduction of different organic spacer layers causes stacking changes in the inorganic layers, which leads to an increase in the optical absorption difference and increment exciton binding energy. Crystal mismatches in 2D polycrystalline films can limit the performance of solar cells: the anisotropic carrier transport property of 2D perovskites inhibit effective charge collection in solar cells when the films are laid flat on a substrate. These defects, mainly caused by the repetition of organic spacer cations, are the origin of the poor PCE of two-dimensional perovskites [34-36].

The constructing 2D/3D heterostructures can effectively improve carrier transport and thus efficiency, while the 2D perovskites with high stability are covered top of 3D perovskites, which serve to protect the 3D perovskites from water erosion with passivating defects, thus improving the cell humidity stability. In 2014, Smith et al. [37] reported that layered perovskite $(PEA)_2(MA)_2[Pb_3I_{10}]$ (1;PEA = $C_6H_5(CH_2)_2NH_3^+$) acted as an absorber in solar cells with an open-circuit voltage of

1.18 V and a PCE of 4.73%. The layered structure offers greater tunability, which may provide additional pathways for material optimization. In 2018, Lin et al. [38] reported the reaction of n-butylamine (BA) with 3D perovskites surfaces to construct 2D/3D stacked structures. The introduction of a thin 2D perovskite layer at the surface and/or grain boundaries of the 3D perovskite enhances the thermal stability of the photovoltaic device. In addition, the thin 2D layer has defect passivation and defect healing effects, which reduce the trap density and extend the carrier lifetime, resulting in an increase of PCE to 19.56%. Currently, Zheng et al. [39] discrete 2D $PEA_2PbBr_{0.3}I_{3.7}$ crystals were covered on top of 3D $MAPbBr_{0.3}I_{2.7}$ films. These discrete 2D $PEA_2PbBr_{0.3}I_{3.7}$ crystals can improve the water resistance by hydrophobic 2D $PEA_2PbBr_{0.3}I_{3.7}$ without sacrificing the photovoltaic performance of 3D $MAPbBr_{0.3}I_{2.7}$. 2D $PEA_2PbBr_{0.3}I_{3.7}$ crystals can increase the embedded potential of PSCs and suppress the interfacial carrier complex, and the final power conversion efficiency reached over 23%. Zhang et al. [40] also utilized the engineered components of guanidine halide (GuX, X=Cl,Br,I) salts for GuCl block treatment and GuI surface treatment, respectively. The dual (bulk and surface) guanidine halogenated treatment based passivation method reduced the carrier losses of block perovskites and extended the long-term stability by preventing the decomposition of the surface structure. The passivation inhibits non-radiative complexation, as well as enhances stability by preventing halogen precipitation. The 2D/3D perovskite has a better long-term stability and a significantly higher efficiency. It provides a feasible method for the high efficiency and long-term stability of the perovskite films and a reasonable design strategy for the overall and surface treatment

of the perovskite films. Sidhik et al. [41] reported a solvent design principle that realizes the longitudinal double-layer stacking of solution-treated 2D/3D perovskite heterojunctions by growing pure phase 2D halide perovskites with different film thicknesses, n values and other parameters on 3D perovskites, obtaining a photoelectric conversion efficiency of 24.5% and super stability of T_{99}>2000 hours. In recent times, the focus of the review of 2D/3D perovskite based solar cells has been on their properties and characteristics, advantages as well as problems and challenges in terms of their long-term stability and device performance [42-46]. Our work involves summarizing the realization of various 2D materials grown on different 3D perovskite surfaces using different techniques over the years. This includes their role towards the formation of heterojunctions and acting as passivation layer. Finally, we highlight the challenges and prospects of applying 2D materials and 2D perovskites on 3D perovskites, providing insights for further performance enhancement and future practical applications.

2. Crystal structure of perovskite

The term perovskite originally referred to a natural crystalline ore with the chemical formula ABX_3, where A is the larger size atom (standing aspect coordination) and B is the smaller atom. Replacing the A-site cation with a large size organic ion in the 3D perovskite structure, the inorganic layer of lead-halogen octahedra will be separated. Due to the void in the inorganic framework is too small to accommodate the larger size organic amine cation, the inorganic layer of lead-halogen octahedra will be

separated and forced to extend in certain directions, forming 2D and quasi-2D low-dimensional perovskites. And the combined effect of quantum confinement and dielectric restraint causes carrier recombination, which is due to the alternating stacking of organic and inorganic layers in the 2D perovskite, forming a natural quantum well structure (Fig. 1a) [47, 48]. The 2D perovskites can be classified into three categories based on the orientation of the inorganic layer BX_6 octahedra (Fig. 1b), among them, the 2D perovskites with <100> orientation are the most diverse [36, 49]. Its structural general formula is $(RNH_3)_2(A)_{n-1}B_nX_{3n+1}$ or $(H_3NRNH_3)(A)_{n-1}B_nX_{3n+1}$, where $[(A)_{n-1}B_nX_{3n+1}]^{2-}$ is derived from 3D perovskites, RNH_3^+ and $(H_3NRNH_3)^{2+}$ represent amine ions, and n indicates the number of layers of BX_6 octahedra between two adjacent layers of amine ions. When n=1, it is 2D perovskites; when $n\rightarrow\infty$, it is 3D perovskite structure; when $1<n\leq10$, the corresponding perovskite is called Ruddlesden-Popper (RP) type perovskite. The value of n continues to increase or different n values exist inside, the corresponding perovskite is called quasi-2D perovskite, the adjacent lamellae in R-P phase 2D perovskites [33, 50].

From the crystal structure, it can be observed that the inorganic layers have relatively staggered configuration, and the R-P phase 2D perovskite usually shows an in-plane displacement of (1/2, 1/2) along the plane of the inorganic layers, showing a large deformation of the inorganic layers, while the D-J phase usually does not have a relative displacement, and the ACI phase is in between, with a relative displacement of (1/2,0) [51, 52]. Among the above three types of 2D perovskites, the R-P phase is the most widely studied, followed by the D-J phase, and the ACI phase is the least. In this

paper, they are referred to 2D perovskites regardless of the n-value.

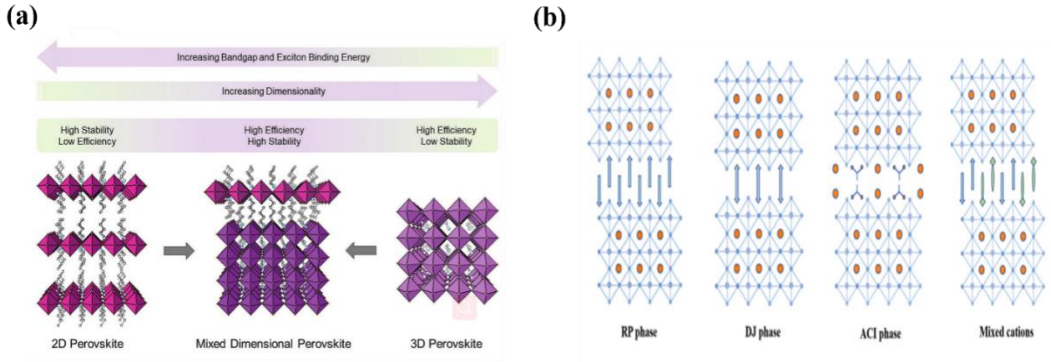

Fig. 1 a Schematic representation of optical, electronic and stability properties of the perovskites based on their dimensionality [36]; **b** Schematic diagram of RP phase, DJ phase, ACI phase and mixed cation phase with multiple cations [32]

2.1 2D RP phase perovskite and solar cells application

2D halide perovskites have good water stability and easy film formation than the 3D perovskites due to their larger exciton binding energy, stronger quantum-limited effects, unique intercalation structure and good crystallization kinetics [34, 53]. The general formula for R-P type organic-inorganic hybrid perovskite is $P_2A_{n-1}B_nX_{3n+I}$, where P is a monovalent organic cation; A is a monovalent cation (e.g. $CH_3NH_3^+$ and $CH(NH_2)^{2+}$) and P is a larger monovalent organic ammonium cation than A. Structurally, when P is a monoamine cation, the terminal amine group interacts with the inorganic halide anion layer by hydrogen bonding, while the adjacent carbon chains of the organic cation are held together by van der Waals forces. When P is a double amine cation, the two terminal amine groups form an insulating layer by hydrogen bonding to the inorganic layer. In 2D PSCs there are a number of aliphatic alkylammonium cations (e.g. propylamine [54] and butylamine [55, 56]), aromatic alkylammonium cations,

(e.g. phenylethylamine [57], 1-(acetylammonio) pyrene [58, 59], and benzimidazolium iodide [60,61]) and thiophene salt cations(e.g. 2-thiophenemethylammonium [62]) used as spacer cations. The complexity of the aromatic cations allows the spacer molecular orbitals to match the energy band structure of the inorganic layer, with the highest occupied molecular orbital (HOMO) and lowest unoccupied molecular orbital (LUMO) of the organic spacer layer being closer to the valence band maximum (VBM) and conduction band minimum (CBM) of the inorganic layer, which can improve charge transport between them (Fig. 2a) [49, 63].

The two-dimensional perovskite crystallization process involves different degrees of $[BX_6]^{4-}$ octahedral aggregation and random orientation resulting in disordered phase arrangement [64], and the resulting multi-n-valued low-dimensional phases have different $[BX_6]^{4-}$ distortion at B-X-B [65] angles, resulting in the accumulation of lattice strain at the interphase boundary, disturbing to the long-range order of the perovskite lattice [66]. The disordered multiphase and unexpected lattice strain during film formation will produce boundary traps for non-radiative recombination centers, limiting exciton splitting and carrier transport [67-69]. The strong interaction between long-chain spacers promotes the aggregation of perovskite precursors, organic spacer cations can adjust the structure and properties of two-dimensional perovskites, and the difference in the number of cationic ligands, metal halides and inorganic layers will lead to changes in the crystal structure and optical properties of 2D perovskite materials, which promotes the formation of favorable vertical phase arrangements of different n values in 2D RP perovskite films, so as to realize bandgap tunability, narrowband

emission and broadband emission **(**Fig. 2b**)** [70-72]. Chang et al. [56] used the ionic liquid 1-butyl-3-methylimidazolium iodide (BMI) as an organic spacer in two-dimensional perovskites and fundamentally changed the quantum well structure with a drastic reduction of the interlayer distance to 3.5 Å, enhancing the interaction between the inorganic plates and weakening the quantum confinement effect of the material A new organo-ammonium ion, 2-furfurylammonium ($FuMA^+$), was designed and synthesized as a spacer ion for 2D RP perovskites by Chen, Zheng et al. [73] The furan-based spacer cation, which has never been used to build 2D perovskite solar cells, was used as a spacer ion for 2D RP perovskites. The thin film structure of $(FuMA)_2(MA)_4Pb_5I_{16}$ was optimized by the addition of methylammonium chloride (MACl) to the precursor solution. The two-dimensional perovskite films with MACl addition showed significantly larger crystal size, enhanced vertical orientation, lower defect density and higher charge mobility compared to the perovskite films without MACl addition. Therefore, understanding the relationship between material composition, crystal structure and optoelectronic properties is beneficial for tuning the band gap, charge transport properties and carrier dynamics to fabricate excellent optoelectronic devices.

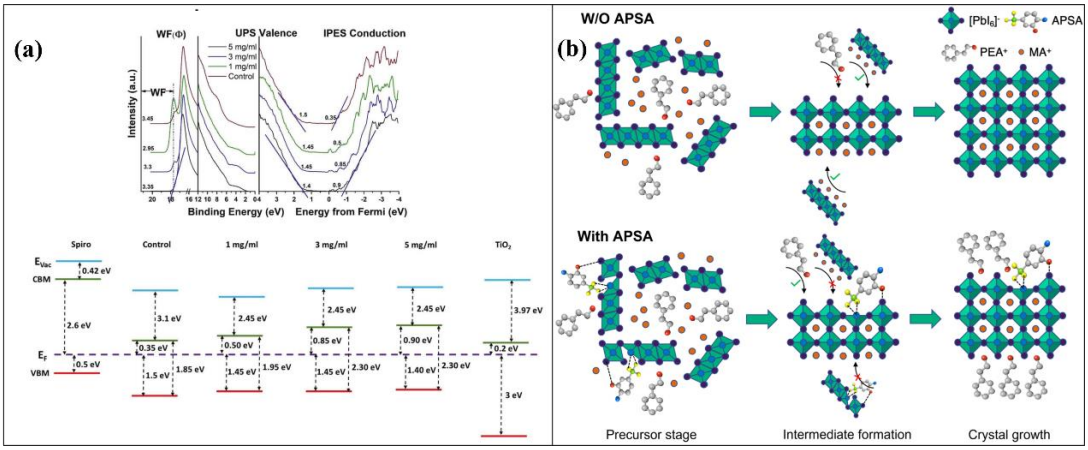

Fig. 2a UPS spectra of perovskite films, illustrating the tuning of energy band diagram between perovskite and TiO_2 ETL and between the VBM of perovskite and HOMO of Spiro-OMeTAD HTL with the incorporation of passivating layers. The presence of long carbon chains of n-BAI modifies the perovskite surface thereby producing valence band shifts that contribute to enhanced hole extraction in passivated devices [55]; **b** Schematic illustration of effect of 3-amino-4-phenolsulfonic acid on the crystal growth of 2D-RPPs, shows that the APSA effectively suppresses the formation of $n \geq 5$ phases and forming n=3 and 4 phases preferentially [70].

2.2 2D DJ phase perovskite and solar cells application

The general formula of D-J type organic-inorganic hybrid perovskite is $PA_{n-1}B_nX_{3n+1}$, where P is a divalent organic cation. As can be seen from the figure 1, the biggest difference between these two types of perovskite is in the relative stacking of layers [74-76]. The organic amine ion P in DJ type perovskite is divalent, so each molecular formula unit only needs one organic amine cation, so it has only one interlaced interlayer cation, and each unit has only one offset layer; The R-P perovskite organic amine ion P is monovalent, so each unit has two offset layers, and there is a pair of interlaced interlayer spacer cations [75, 77]. In general, the weak interaction between adjacent inorganic $[BX_6]^{4-}$ octahedral plates in two-dimensional RP perovskite and the presence of van der Waals gaps in the organic interval do not adequately

289 stabilize their layered structure. In two-dimensional DJ perovskite, due to the use of a
290 spacer layer between adjacent inorganic plates, thereby shortening the distance between
291 plates and eliminating van der Waals gaps.The reduction of the distance between layers
292 and the resulting weakening of the quantum limiting effect and the narrowing of the
293 gap will facilitate the separation and/or transport of electrical charges and the collection
294 of light [78-80].

295 The basic properties of DJ phase and RP phase are similar and are generally
296 determined by bulky organic cations. The properties of DJ perovskites are usually
297 determined by diammonium properties such as positive charge, hydrogen bond energy,
298 size, and stereochemical composition [81-83]. These diammoniums can be classified
299 as linear cations [84]. cyclic cations [85], piperidine cations [86], pyridine cations [87],
300 and thiophene cations [88] **(**Fig. 3**)**. Some aromatic diammonium cations commonly
301 found in the D-J phase, such as pyridinyl aromatic spacers (3AMP, 4AMP) [65, 89-
302 91], aliphatic diamine spacers such as 1,4-butadiemine (BDA) [92] and 1,3-
303 propanediamine (PDA) [93], phenyl aromatic spacers (PDMA) [94] and thienyl
304 aromatic spacers (ThDMA) [88] have been developed as organic spacers in two-
305 dimensional DJ PSCs to improve device performance [95]. Xu et al. [77] developed
306 a fusion thiophenyl spacer, namely thiophene [3,2-b]thiophene-2,5-
307 diyldimethanaminium iodide (TTDMAI), as a block organic spacer for two-
308 dimensional DJ perovskite, which can stabilize the perovskite structure and reduce the
309 dielectric mismatch between the organic layer and the adjacent inorganic layer,
310 compared with the ThDMA spacer, due to the template effect of strong intermolecular

311 interaction, TTDMA spacers with increased π conjugate length can induce crystal
312 growth in the vertical direction and also enhance the structural stability of 2D DJ
313 perovskite in light, heat and environmental aging tests, reducing trap density, exciton
314 binding energy and directional charge transport. Two-dimensional perovskite has great
315 potential in photoelectricity with stability under continuous light, and the ferroelectric
316 and spin-related properties of organic-inorganic hybrid perovskite are also of increasing
317 interest. The presence of strong spin-orbital coupling, coupled with the symmetry
318 breakdown guaranteed by the residual polarization, will lead to Rashba-type cleavage
319 of the electron belt in perovskite. The two-dimensional Dion-Jacobson perovskite is a
320 room-temperature Rashba ferroelectric material, a potential spintronic material, and its
321 robust ferroelectricity and Rashba effects are also more meaningful [76, 96].

322 The ACI phase is between the RP phase and the DJ phase, and chiral alternating
323 cationic intercalation (ACI) perovskite has great structural flexibility and suitable
324 quantum well barrier thickness, which is conducive to better charge transport [97]. Li
325 et al. [98] used 1,4-Butanediamine (BEA) as a mixed cation (FA, MA and Cs) as an
326 interlayer spacer to form a new type of low-dimensional perovskite, constructed a
327 narrowly distributed quantum well width, formed an efficient carrier transport path,
328 effectively reduced the obstacles to charge transport, and made the diffusion length of
329 equilibrium carriers (electrons and holes) exceed 350 nm, the PCE reached 17.39%.
330 Interlayer space (B-ACI) perovskite combines the advantages of ACI and DJ perovskite,
331 but exhibits greater stability under humidity, heating and light immersion. However,
332 there is relatively little research on ACI phase two-dimensional perovskites due to the

infrequent organic spacer, and it is discussed briefly.

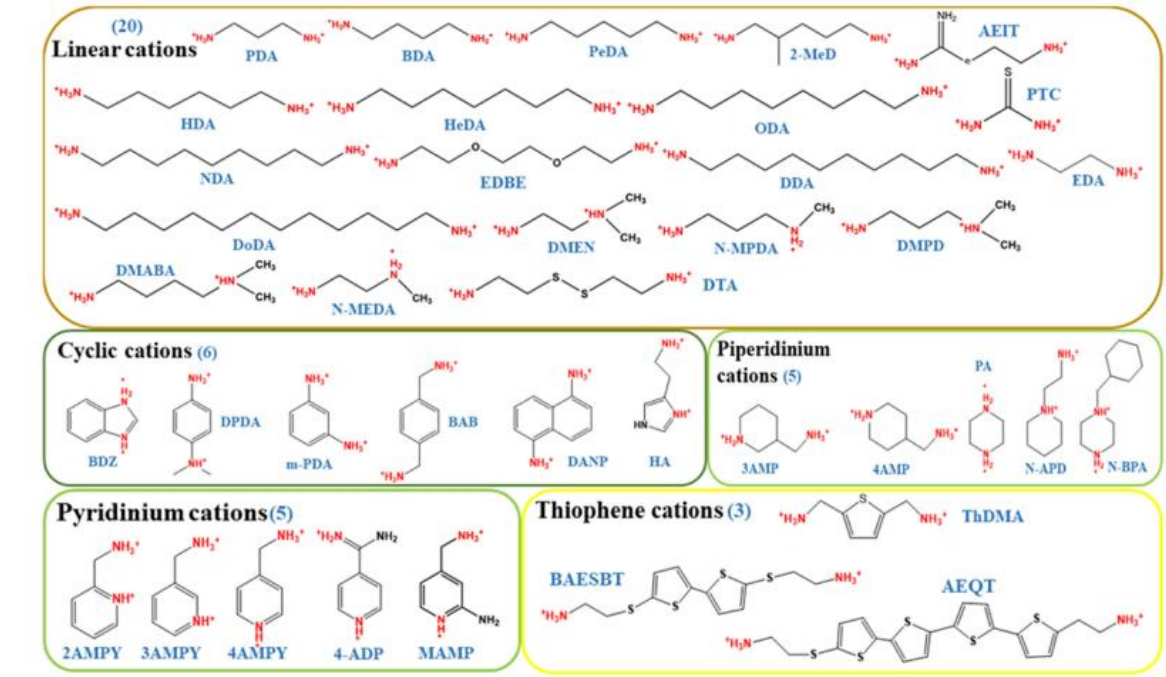

Fig. 3 Different types of spacer cations in DJ phase 2D perovskites [95]

2.3 3D phase perovskite and solar cells application

A typical 3D organic-inorganic hybrid perovskite has the molecular formula ABX_3, and its inorganic framework is composed of octahedra formed with B as the center and halogen atoms as the vertices by co-top connection. It is shown in Fig. 4a, where X is coordinated to B in a $[BX_6]^{4-}$ octahedral structure, and the cation at the A-site is located in the framework cavity. This configuration leads to the formation of a 3D inorganic framework in which the non-bonded A-site cations are embedded in the cuboctahedral framework. The A-site is a monovalent cation with a radius, such as the inorganic metal ion Cs+. Rb+, the organoammonium ion $CH3NH3^+$ (MA) or the formamidine ion $HC(NH2)_2^+$ (FA) [99], the B-site is usually composed of divalent

metal cations with smaller radii, (e.g. Pb^{2+}, Sn^{2+}, Ge^{2+}, etc.) and X is a halogenated anion (e.g. I, Br or Cl, SCN^-), which is usually represented by the Goldschmidt tolerance factor (t). The Goldschmidt is usually used to predict the stability of the perovskite structure and to determine the distortion of the perovskite crystal (as shown in Fig. 4b: $t = \frac{R_A+R_B}{\sqrt{2}(R_B+R_X)}$,where R_A, R_B and Rx are the ionic radii of A, B and X, respectively. The most symmetrical perovskite crystal structure occupies the Pm3m space group in which the ions are perfectly stacked, and the tolerance factor t = l for this class of perovskites, i.e., the A, B and X ionic radii follow the quantitative relationship $R_A+R_X=\sqrt{2}(R_B + R_X)$. When t is in the range of 0.76 to 1.13, the crystal structure of the compound shows an cubic structure, it forms a 3D perovskite structure, while other structures related to perovskite are unstable outside this range [100-102]. The perovskite crystal structure is distorted when the perovskite A-site cations are replaced, especially when the A-site cations are too small (Na, K and Rb) or too large (imidazolium, ethylamonium and guanidinium, etc.) [103]. In addition, the perovskite structure is also constrained by the octahedral coefficient μ, which is defined as: $\mu = \frac{R_B}{R_X}$,where μ describes the stability of the BX_6^{4-} octahedron and is determined by the ratio of the radii of the B- and X-site ions. the stability of μ ranges from 0442 to 0.895. Tolerance and octahedral factors are currently used to predict the stability of novel possible perovskite compositions. Many of the properties of perovskites are affected by structural deformation, so that partial or full cation as well as anion substitution can be used to modulate the physical properties. In general, the A-site cation is highly ionized and contributes little to the band gap edges; therefore, the $[BX_6]^{4-}$ octahedral

structure composed of B and X directly determines the energy band structure of perovskites. Alternatively, we can describe the symmetry of perovskites by the interaction forces between the organic A- and X-site [104]. The specific arrangement of the A-site organic cations is caused by hydrogen bonding in the perovskite lattice, and the order of this electron depends on the dipole moment of the A-site and the strength of the hydrogen bond, and the disordered A-site organic cation alter hydrogen bonding to affect symmetry. Organic cation MA has an electric dipole of 2.3D, which affects its characteristics and performance in perovskite solar cells [105]. Inorganic metal cations at the B-site are usually selected for Pb^{2+}, the Pb outer electronically strong off-domain, and the perfect coupling of halogens contribute to the current optimal B-site. However, due to the greater toxicity of lead, people are also looking for other safer and more environmentally friendly materials while improving lead leakage [86]. The choice of B-site metal cation affects the size of the perovskite structure, especially when the metal cation is trivalent and tetravalent. The band gap of perovskites varies with the alternation of anions (usually I or Br) and the mixing of anions, which is associated with the lower electronegativity of smaller halogen atoms. Therefore, it is easy to modulate the light absorption in the visible spectral range by bandgap engineering of halogenated perovskites. The small organic cations that can be well inserted into the inorganic framework are MA^+ and FA^+, which are common today. Among them, FA^+-based 3D perovskites are the most common and have many unique properties such as phase transition or light absorption. Currently, such perovskites are often used as photoactive layers in solar cell devices due to their better

light absorption properties and band gap (1.5 eV) close to the optimal efficiency of solar cells. Liu et al. [106] prepared efficient and stable $(CsPbI_3)_{0.05}[(FAPbI_3)_{0.97}(MAPbBr_3)_{0.03}]_{0.95}$ PVKs. In addition to reducing the under liganded trap states associated with Pb^{2+} ions by forming interactions with functional groups, the complex layers readily form dipole moments and enhance the internal electric field, thus facilitating carrier extraction, obtaining a maximum efficiency of 23.55% and neglecting hysteresis. Tian et al. [107] introduced in the perovskite layer 2-[N,N-bi(trifluoromethylsulfonyl)amino]pyridine (2-BTFSIP) integrated additive in which sulfonyl and pyridine nitrogen synergistically passivated deep energy level traps (Pb^0 clusters and undercoordinated Pb^{2+} ions), while trifluoromethyl inhibited the evaporation of organic cations and improved the hydrophobicity of the perovskite film. The $MAPbI_3$ and $FAPbI_3$ devices passivated by 2-BTFSIP molecules obtained appreciable efficiencies of 21.96% and 22.90%, respectively.

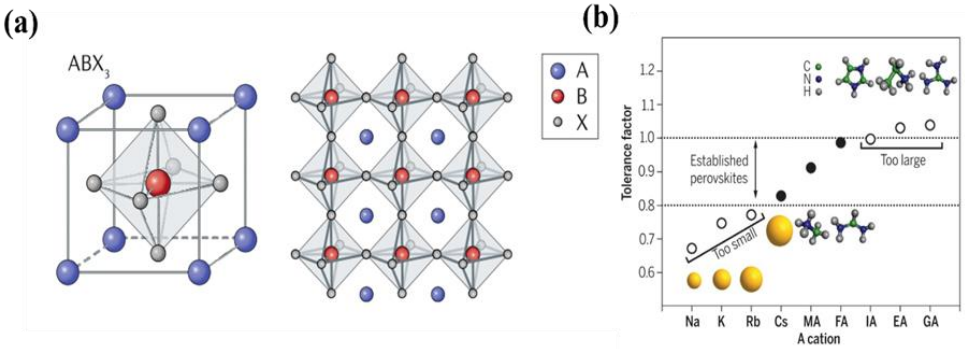

Fig. 4 a Crystal structure of perovskite materials. Reproduced with permission [108]; **b** Tolerance factors of perovskite corresponding to different A-site cations [37]

3.2D/3D organic-inorganic hybrid perovskite

The recorded power conversion efficiency (PCE) of pure two-dimensional

perovskites (~ 20%) is still much lower than that of three-dimensional perovskites (25.7%) [2]. This bottleneck stems from two main problems: 1) the long chain spacer molecules between inorganic octahedra hinder exciton splitting and interlayer charge transport; 2) the randomly oriented two-dimensional lattice hinders charge transport along the working direction in the device. But the high efficiency of three-dimensional perovskites with surface defects and instabilities are also great problems, such as easy decomposition in humid environments, chemical MA/FA/I element vacancies and incongruent lead halide clusters, and MA or FA cations with small radii and low formation energies have high degrees of freedom within the lattice, making it easy for ions migration under thermal/electric fields [36]. However, 2D perovskite thin layers can also be formed as interfacial layers on preformed 3D perovskites to facilitate charge selection at external electrodes, and such 2D capping layers can passivate the surface defects of 3D perovskite absorbers, resulting in perovskite absorbers with low defect density and long carrier lifetime [109]. The stability can also be greatly improved due to the high hydrophobicity of the two-dimensional perovskite capping layer, and the efficiency of the two-dimensional perovskite grows gradually with the assistance of the three-dimensional perovskite.

3.1 Water resistance and growth orientation control

Two-dimensional perovskites can inhibit water penetration and limit ion migration due to the hydrophobicity of organic cations. The degradation of perovskites is prevented, thus improving stability under harsh moisture conditions [82, 110, 111]. Bhushan P. Kore et al. [112] studied three organic cations with different alkyl chain

lengths, using highly resistant alkylammonium cationic lead iodide perovskites ($(C_nH_{2n+1}NH_3)_2PbI_4$(n = 14, 16 and 18) as the encapsulation layer on top of the light-absorbing FA/MA cationic 3D perovskite, and the perovskite film can be maintained for three minutes after being completely immersed in water, and the hydrophobicity is greatly improved. After 60 days of exposure to ambient conditions of 25-80% relative humidity (RH), the diffraction peak of the XRD image of the 2D/3D perovskite film did not change much. It not only encapsulates three-dimensional perovskites, but also acts as a passivation layer, significantly reducing recombination losses **(**Fig. 5a**)**. 2-Trifluoromethyl-phenylethylamine hydroiodide (2-CF_3-PEAI) is used as a multifunctional trap inactivation reagent, which can react with metallic lead to eliminate deep energy-level Pb^0 traps, forming a thin layer of 2D perovskite (2-CF_3-PEA)$_2PbI_4$ on top of 3D perovskite without blocking carrier transport. The resulting 2D perovskite can hinder the diffusion of Ag to 3D perovskite, thus slowing down the formation of silver iodide. Due to the strong electron-absorbing and hydrophobic nature of trifluoromethyl, it can significantly change the dipole moment and polarity of phenylethylamine iodide (PEAI), which in turn prevents the penetration of water molecules and forms a waterproof protective layer, thus improving efficiency and stability. Similarly, 1,8-naphthopyridine (1,8-ND) was used as an interfacial modification material between the calixarene/HTL (hole transport layer) films [113], forming a two-dimensional calixarene with reduced defect density, extended carrier lifetime, good hydrophobicity, and α-$FAPbI_3$ phase becomes inhibited in the optimized calixarene films, and after 50d, the optimized equipment maintained 83.2% of the initial

PCE higher than the control of 46.3%, showing good environmental stability (Fig. 5b). Zheng et al. [39] also reported that hydrophobic two-dimensional $PEA_2PbBr_{0.3}I_{3.7}$ crystals discretely cover 2D/3D PSCs on top of three-dimensional $MAPbBr_{0.3}I_{2.7}$ films, and these discrete two-dimensional crystals improve water resistance without sacrificing the photoelectric performance of 3D $MAPbBr_{0.3}I_{2.7}$.

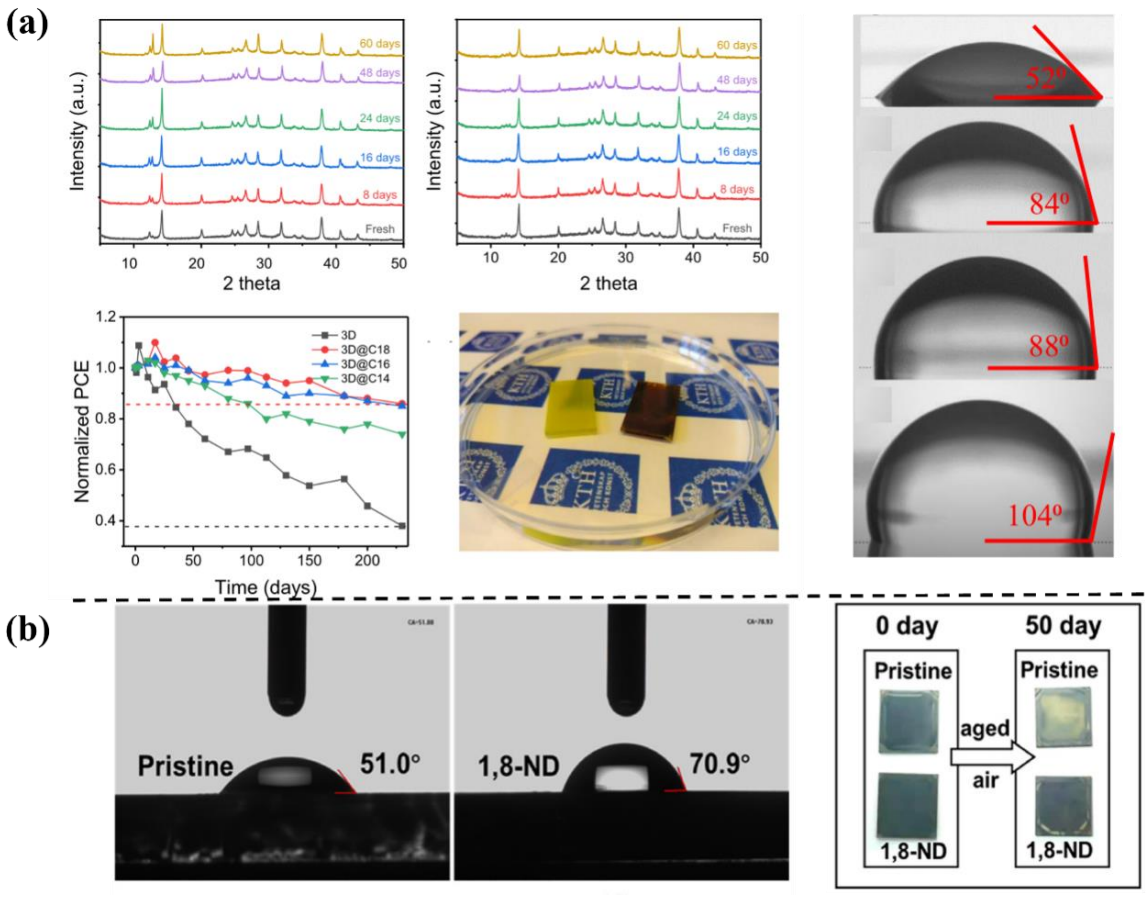

Fig. 5 a XRD images before and after optimization and improvements in hydrophobicity and stability. Reproduced with permission [112]; **b** Water contact angle and changes in the film after 50 days of air before and after 1,8-NDs treatment [113]

Yu et al. [114] introduced 4-fluorophenylethylammonium iodide (FPEAI) bifunctional agent in the experiment, with FPEAI as an additive in the precursor, to

promote (100) oriented optimal growth and improve crystallinity. Compared with the control film, the additive film provides a high ratio of (100) planes, (100) and (200) reflected peak intensities significantly increased, especially (100) peaks, further demonstrating the optimal orientation of the grain direction (100) direction after the addition of FPEAI,and the surface energy changes during crystal growth. At the same time, the unit cell expansion caused by the incorporation of large alkylammonium ions in $FPEA^+$ into the broad-gap perovskite in the perovskite lattice also slightly shifted the (200) peak position, and the PCE of the wide-bandgap solar cells reached 19.07%, while the voltage loss was relatively less. In addition to improving the hydrophobicity of the device and increasing the stability of the device, the addition of the two-dimensional perovskite layer can regulate the growth orientation of the crystal, which is more conducive to carrier movement, thus improving the device performance.

Liu, Gao et al. [115] have researched and developed a class of FA-based aromatic formamidine (ArFA) derivatives such as benzamidine hydrochloride (PhFACl), 4-hydroxybenzamidine (p-HOPhFACl), and 4-fluorobenzamidine (p-FPhFACl) for 2D/3D mixed PSCs. Due to the addition of the ArFA spacing, the crystal part is reoriented with preferential vertical orientation relative to the substrate, resulting in a preferentially oriented 2D/3D hybrid perovskite, while reducing the defect state and expanding the spatially resolved carrier lifetime. And there are multiple NH···I hydrogen bonding between the large aromatic spacer ArFA and the inorganic $[PbI_6]^{4-}$ layer in 2D/3D perovskite. After the improvement of the organic salt, benzamidine hydrochloride (PhFACl), the efficiency is significantly improved, and by further

optimizing the perovskite film, the final 2D/3D device champion efficiency reaches 23.36%, which is one of the most efficient devices of 2D/3D hybrid PSCs. At the same time, PhFACl-based devices have high thermal stability, and these results indicate that ArFA spacing may be an excellent class of spacer materials with great potential for efficient 2D/3D PSC perovskite solar cells.

Uzurano et al. [116] used the "double-rod coating method" to prepare 2D/3D perovskite heterostructures.The $MAPbI_3$ precursor solution is first coated on the matrix, and the second coating converts the 3D perovskite in the top layer to 2D perovskite. When isopropanol (IPA) solution of ammonium butyl iodide (BAI) was coated at 80 ° C, MAI in perovskite film was replaced by BAI to form 2D/3D heterostructures. The liquid film of the precursor solution is converted into 3D perovskites by a subsequent annealing process. The solvent and precursor stoichiometry ratio of the thin film precursor determines the crystal orientation of the three-dimensional perovskite. Fig. 6a-f shows the grazing-incidence wide-angle X-ray scattering (GIWAXS) mode of 2D/3D heterostructures constructed on $MAPbI_{2.5}Cl_{0.5}$ in the tequal (110) orientation and $MAPbI_3$ in the (200)/(112) orientation, the substrate diagram, the azimuth angle χ profiles of the heterostructure at Q = 3.15 nm^{-1}, respectively. The curved patterns of $BA_2MAPb_2I_7$ (n=2) and $BA_2MA_2Pb_3I_{10}$ (n = 3) octahedral plates were observed, which proved the existence of directional two-dimensional perovskites. The two-dimensional perovskite quantum well prepared on (110) oriented $MAPbI_{2.5}Cl_{0.5}$ forms horizontally along the substrate surface. The diffraction peak of $BA_2MAPb_2I_7$ octahedral sheet is located at 45° from the Q_z axis, that is, (200)/(112)-oriented 3D perovskite behaved as

a template,then the orientation of 45° in 2D perovskite appeared, and their orientations are completely different. The half-width of the orientation peak of (200)/(112) seems narrower than that of (110). Therefore, 2D perovskite is prepared on 3D perovskite with directional control, which realizes the directional control of 2D perovskite and improves the stability of perovskite solar cells. In addition, the template growth is tolerant to different lattice spacing between 2D and 3D perovskites. Therefore, this directional control method can also be applied to other types of 3D perovskites.

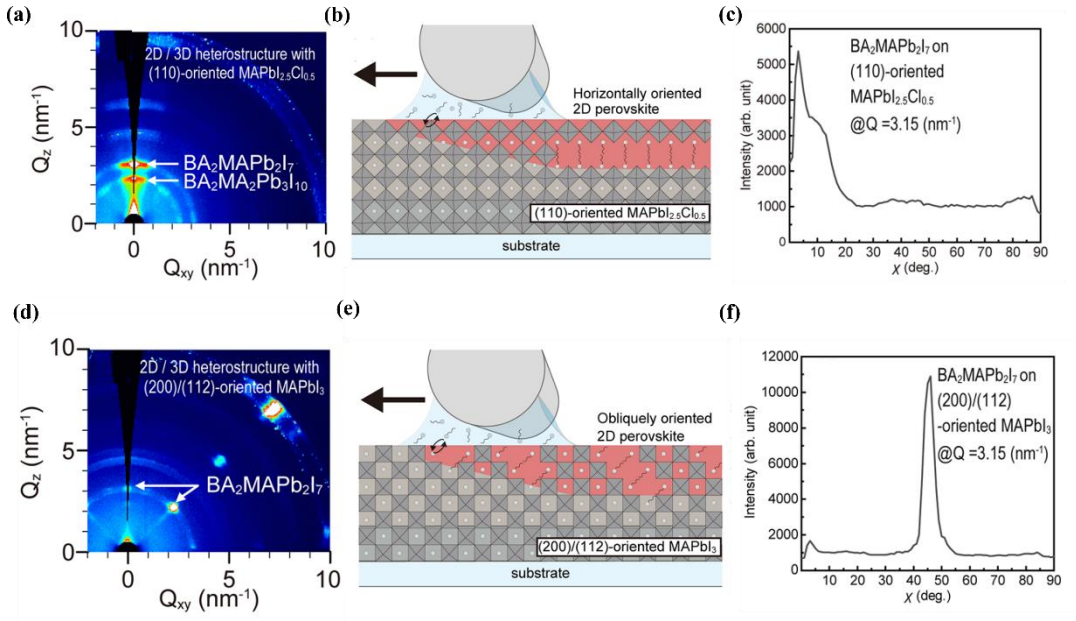

Figure. 6 a,d the GIWAXS pattern of 2D/3D heterostructure constructed on different orientations; **b,e** Schematic diagram of two-dimensional perovskites with different orientations(horizontally and oblique); **c,f** the χ profile at Q = 3.15 nm^{-1} of heterostructure fabricated on different orientations. [116]

3.2 Band arrangement

Xiong et al. [117] proposed a generalized precrystallization method in commonly used RP phase perovskites to control the phase purity during the formation of 2D/3D

bulk heterostructures by introducing 2D perovskite crystals with rigid π-conjugated. By introducing chloride 2D perovskite $(PYA)_2PbCl_4$ (PYA = ammonium propargyl) crystals into the 3D precursor solution, 2D/3D heterojunction with a clear type I band arrangement was achieved, which greatly reduced charge recombination. Moreover, the addition of alkyne perovskite also showed inhibition of iodine diffusion due to its special iodine trapping ability. The obtained 2D/3D heterostructure devices have higher efficiency and stability than the 3D heterostructure devices. Due to their large lattice mismatches with inorganic components and organic cations, we are able to suppress the phase transition and preserve the original 2D perovskite (n = 1) phase. Combined with these features, the efficiencies of MA-Free and CsFAMA inverted PSCs reached 21.6% and 22.7%, respectively. It can also be seen from transient absorption (TA) spectra that the large lattice mismatch caused by Cl/I halide difference and rigid ligand imbed the retained pure 2D perovskite (n = 1) on grain boundaries (GB). The retained pure 2D phase in the heterojunction not only passivates the defect site at GB, but also establishes the electron-clean type I heterostructure to improve carrier collection. Thus, PSCs with high quality 2D/3D junctions show a significant increase in efficiency and lifetime, as shown in Fig. 7a,b.

Jeong et al. [118] introduced the novel two-dimensional layered perovskite CHA_2PbI_4(CHAI = cyclohexylammonium iodide) and $CHMA_2PbI_4$ (CHMAI = cyclohexylmethylammonium iodide) between the $FAPbI_3$ three-dimensional perovskite and the hole transport layer through a simple solution process, which improved the performance of PSCs by forming a funnel-like band arrangement and effective charge

552 transport, and confirmed the formation of two-dimensional/three-dimensional
553 perovskite heterojunctions. CHMAI is dissolved in IPA solution to form a thin layer of
554 two-dimensional perovskite. As shown in Fig. 7c, the resulting film contains an
555 increasing number of cationic components. Based on the out-of-plane profiles of the
556 CHMAI-treated perovskite films in GIWAXS, crystallographic information proving the
557 gradual change of the layers can be observed (Fig. 7d). $FAPbI_3$ (α), $CHMA_2PbI_4$ (#)
558 and PbI_2 (+) peaks are evident. Observe the XRD spectrum of film in different $FAPbI_3$
559 and $CHMA_2PbI_4$ ratios (&) Fig. 7f. Here it is thought that a new gradient layer has
560 appeared. And according to the relationship between the depth of X-ray penetration and
561 the angle of incidence, by calculating the ratio of the peak integration area of
562 $CHMA_2PbI_4$ and $FAPbI_3$, the thickness of the gradient layer was carefully estimated as
563 ≈13 nm, as shown in Fig. 7d. The presence of a gradient layer in a 2D/3D heterojunction
564 (Fig. 7e) enables efficient funnel-shaped band alignment, making hole
565 separation/transport in PSCs more efficient. Severe voltage losses in wide bandgap
566 (PSCs) have a significant impact on the enhancement of PV performance. Yu et al. [114]
567 used 4-fluorophenethylamine ammonium iodide (FPEAI) as a bifunctional agent for
568 directional crystallization and comprehensive passivation of WBG perovskite
569 $Cs_{0.2}FA_{0.8}Pb(I_{0.7}Br_{0.3})_3$. The addition of FPEAI promotes crystal growth in the (100)
570 direction, improves the crystallinity, induces the matching energy level arrangement,
571 promotes hole transport, inhibits non-radiative recombination, and reduces voltage loss
572 limits the enhanced photovoltaic performance.

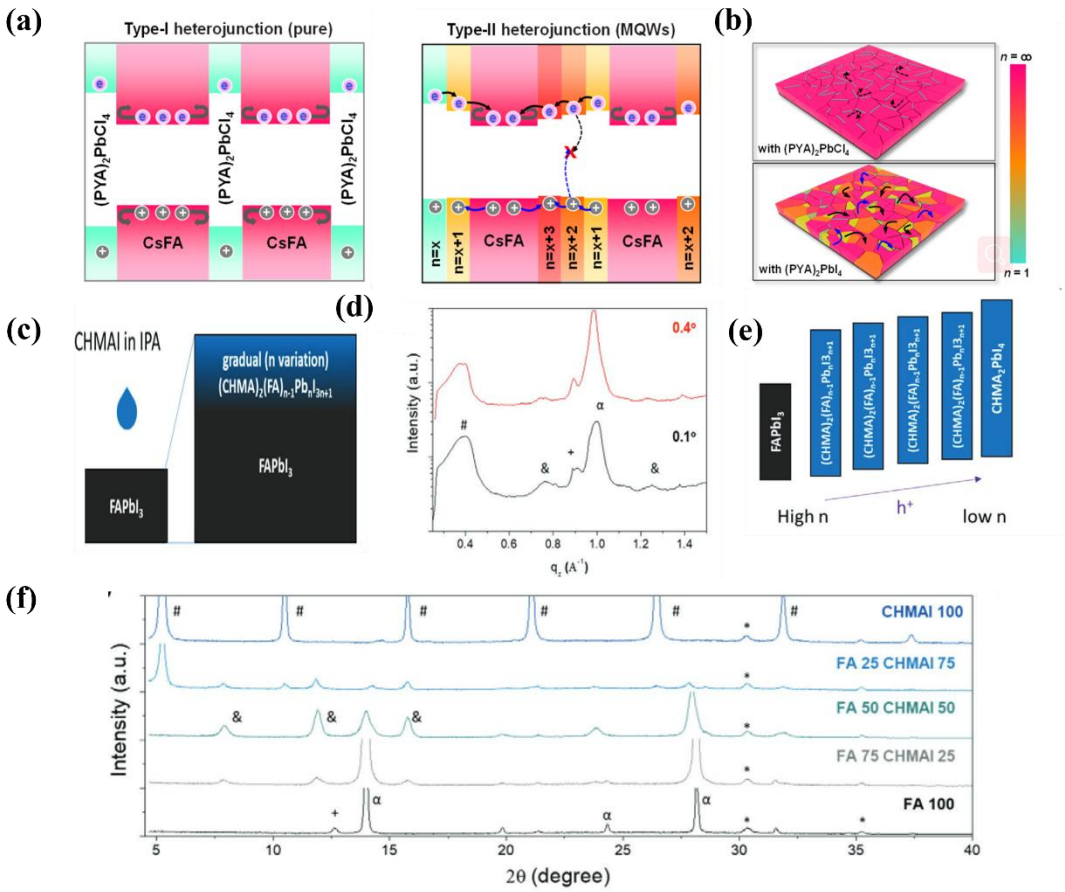

Fig. 7 Illustration of **a** energy alignment and **b** charge transfer process in 2D/3D perovskite films having different 2D phase [117]; **c** Schematic illustration of CHMAI treatment; **d** Out-of-plane line profiles of CHMAI treated perovskite film; **e** Energy-level alignment in $(FAPbI_3)_x(CHMA_2PbI_4)_{1-x}$ perovskite films; **f** X-ray diffraction pattern of $(FAPbI_3)_x(CHMA_2PbI_4)_{1-x}$ Films (* – ITO (internal reference)) [118]

3.3 Heterojunction

The two-dimensional organic long-chain cation is mixed with the three-dimensional perovskite precursor solution, spin coated [119], and the 2D/3D heterojunction structure is prepared by component engineering, or the 2D precursor solution or long organic chain cation is spun-coated on the initially formed 3D perovskite film by using interface engineering [120] to form a 2D/3D heterojunction to reduce surface defects. For example, a 2D perovskite with a wide bandgap is overlaid

587 on a 3D perovskite to form a 2D/3D perovskite heterojunction, but the electrical
588 insulation of large-size organic cations makes the charge transfer in the two-
589 dimensional perovskite limited by long-chain organic ligands, causing an obstacle to
590 the transfer of charge from the 2D/3D heterojunction to the hole transport layer. Since
591 high-n-value 2D phases are prone to the formation of out-of-plane accumulation of
592 inorganic layers, efficient carrier transport pathways can be created by increasing the
593 number of high-n-value (n≥3) 2D phases and reducing the number of unwanted n=1
594 and n=2 2D phases, which is more conducive to improving efficiency [121-123]. For
595 increasing PCE, according to the Shockley-Queser (S-Q) model, increasing the open-
596 circuit voltage (V_{OC}) is one of the effective means to obtain high-performance batteries
597 [124, 125]. On the one hand, band mismatch between the perovskite layer and the
598 charge transport layer leads to charge recombination and V_{OC} loss. The charge
599 recombination loss due to trap defects can also deviate V_{OC} from the radiation limit (Fig.
600 8a). V_{oc} is closely related to non-radiative recombination, for which we often choose
601 defect passivation as one of the methods. 2D perovskites with wider bandgaps provide
602 defect-free interfaces and modifiable bands that minimize charge recombination in the
603 interface region. In situ growth of two-dimensional perovskites to form two-
604 dimensional/three-dimensional heterojunction PSCs is a feasible method to inhibit
605 high-PCE non-radiative recombination, which can effectively improve long-term
606 stability and minimize V_{OC} loss and defects (Fig. 8b) [126-129].

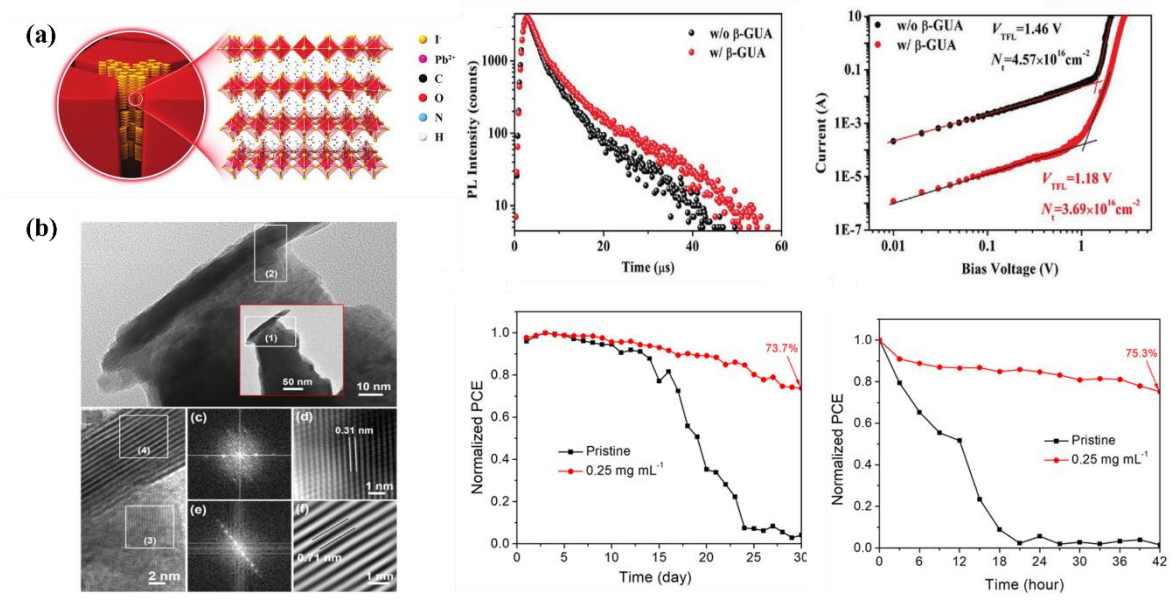

Fig. 8 a The crystal structure of two-dimensional perovskite at n=1, steady-state photoluminescence (PL) spectra and trap filling limited voltage (V_{TFL})I-V curves of the pristine and β-GuA-doped $FA_{0.95}Cs_{0.05}PbI_3$ PVSCs are shown, non-radiative recombination is inhibited [128]; **b** TEM and HRTEM images of $MAPbI_3$ treated by the 0.25-$DMEDAI_2$ solution, confirming the formation of 2D/3D heterojunctions. Humidity and heat stability and photostability [59]

He et al. [130] used long alkyl chain dodecylammonium bromide (DABr) and excess PbI_2 to react preferentially on the grain boundary of metal halide perovskite, and designed a two-dimensional perovsky with matching energy level and high stability on the three-dimensional perovskite surface to form DA_2PbI_4(n = 1), and the ion exchange between Br and I further promoted the formation of 2D perovskite and formed a clear 2D/3D heterojunction. The presence of a heterojunction increases the strength of the device's built-in electric field, enhances the separation and extraction of carriers, and the amino passivation of dodecylammonium cations imperfections reduces the non-radiative rebinding of the carrier, increasing the power conversion efficiency (PCE)

624 from 20.35 to 21.81%. Embedding special functional groups into spacer molecules can
625 not only give full play to the positive influence of spacer molecules on the structure and
626 photoelectric properties of two-dimensional perovskites, but also provide a feasible
627 method for constructing stable and hysteresis-free 2D PSCs overlays. Fan et al. [131]
628 successfully prepared 2D/3D heterojunctions by dissolving the customized spacer
629 molecule 4-hydroxyphenylethylamine iodide (OH-PEAI) in IPA solution and then
630 applying it to the prepared 3D perovskite membrane after post-treatment. The three-
631 dimensional surface two-dimensional structure based on OH-PEAI significantly
632 reduces the defect density and slows down the non-radiative recombination. The open-
633 circuit voltage (V_{OC}) is as high as 1.234, the Voc loss is only 0.376V, and the hysteresis
634 is almost completely gone.

635 Jang et al. [132] Stable highly crystalline 2D $(C_4H_9NH_3)_2PbI_4$ films were grown
636 on 3D films by applying pressure and heat using solvent-free solid-phase plane growth
637 technology to prepare complete 2D/3D heterojunction. As a result, the built-in potential
638 is enhanced and a higher optical voltage is generated in the device. The solid-phase
639 planar growth technique successfully avoids unintended phase formation, and the
640 thickness of the controllable 2D layer helps to optimize the device, increase the built-
641 in potential at the junction, and maximize stability. (Fig. 9a-c) (GIWAXS) can be seen
642 to produce a quasi-two-dimensional, solid-state planar growth film with an undefined
643 phase growing a uniform and complete 2D/3D bilayer film across the entire surface.
644 Tauc plots of UV-electron spectroscopy data and UV-vis absorption spectra in Fig. 9e
645 estimate the position of each band of the 2D and 3D films and the work function of 4.92

eV, demonstrating a wider bandgap of $(BA)_2PbI_4$, reaching 2.38 eV. The inline potential change caused by the formation of two-dimensional/three-dimensional heterojunctions in Fig. 9f, the depletion region depends on the carrier concentration of the two-dimensional layer, increasing the thickness of the two-dimensional layer can add additional V_{bi} by further ensuring the depletion region in the two-dimensional layer, and a thicker intact two-dimensional layer is expected to provide higher photovoltaic performance for the PSCs obtained by the solid-phase planar growth technology process. The complete 2D/3D heterojunction results in an open-circuit voltage of 1.185V and a steady-state efficiency of 24.35%. After 1056 h of humid heat test (85°C/85% relative humidity), the initial efficiency of the packaged device remained at 94% and 98% after 1620 h of full sunlight.

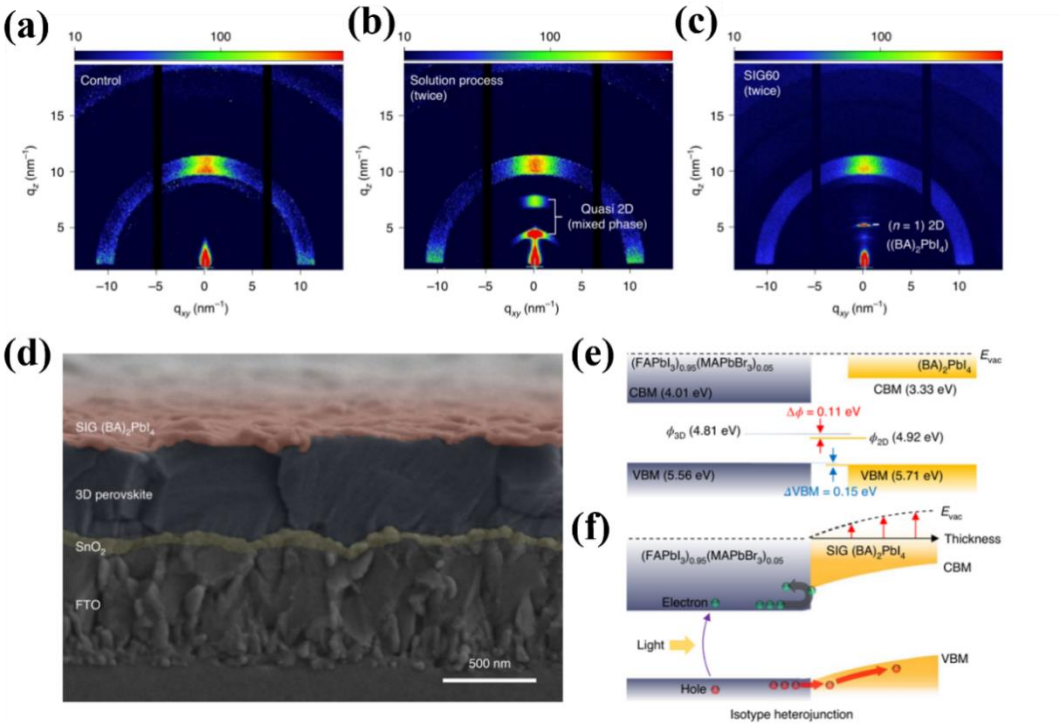

Fig. 9 a–c GIWAXS images of control, solution method and SIG process; **d** A cross-sectional SEM image of the SIG-processed 2D/3D perovskite based device; **e** Energy-level alignment between the

3D perovskite and $(BA)_2PbI_4$; **f** Built-in potential change induced by the formation of 2D/3D heterojunction [132]

Chen et al. [133] used interface engineering strategies to prepare inverted wide bandgap PSCs ($FA_{0.8}Cs_{0.2}Pb(I_{0.8}Br_{0.2})_3$), with a band width of about 1.68 eV, and low Br content in wide bandgap perovskite absorbents, which was conducive to alleviating halide phase segregation [134]. The formation of a thiophene-based 2D/3D perovskite heterojunction interface using 2-thiopheneethylammonium chloride (TEACl) passivates the defects of the surface and grain boundaries of the wide bandgap perovskite film, in which the presence of thiophene and ammonium groups passivates the defects of positive and negative charges in the perovskite film (as illustrated in Fig. 10a) [135]. Therefore, the carrier lifetime is extended, the activation energy of ion migration is increased, the dark saturation current density of wide bandgap PSCs is reduced, the V_{OC} defect is reduced, and the performance of solar cells is improved. At the same time, the improvement of hydrophobicity enhances stability against moist heat. The appearance of additional peaks in the XRD image in Fig. 10b shows the formation of 3D/2D perovskites, followed by the apparent photoluminescence (PL) peak in Fig. 10c PL at 538 nm indirectly verifies the formation of 2D/3D heterojunctions. The longest film lifetime at the optimal concentration shown in TRPL also shows the passivation effect of two-dimensional perovskites on surface defects, and the upward shift of the Fermi level increases V_{OC} after TEACl treatment (Fig. 10d).

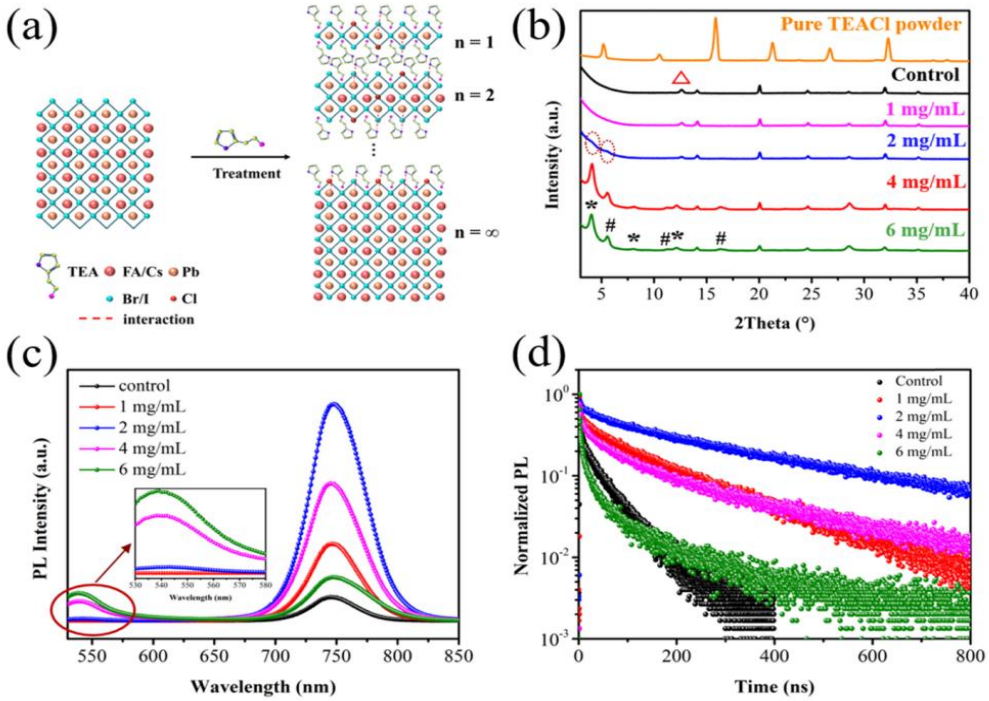

Fig. 10 a The schematic diagram of the 2D perovskite formation with TEACl treatment. **b** XRD patterns of the perovskite films treated with and without TEACl. **c** The steady-state PL spectra and **d** TRPL decay curves of perovskite films treated with different concentrations of TEACl solution [133].

Liu et al. [136] report a gradient dimension engineering that diffuses amphiphilic spaced cations from the interface to matrix construction, while passivating the bulk defects and interface defects of perovskite films, improving pore extraction, etc. The introduction of tert-butyl groups at spacer cations increases the moisture stability of films and devices and contributes to the moisture stability of films and devices. The gradient distribution of 2D perovskites in 3D perovskite films confirms the successful construction of TBHCl-modified gradient 2D/3D heterojunctions, and at the same time, the interfacial band row is improved to promote hole extraction, and the formed wide bandgap 2D perovskites can form Type I heterojunctions, which is conducive to the transport and transfer of carriers and the overall passivation of defects from the surface to the bottom of the perovskite film (Fig. 11a). He et al. [137] introduced isoammonium

iodide (PNAI) with variable alkyl chains without rigid benzene structure as a large organic ammonium salt, which is easy to disperse into the perovskite lattice, which is conducive to the formation of a two-dimensional perovskite phase with high n value (n ≥2) on the three-dimensional surface of perovskite, which is conducive to interfacial charge transfer, and the presence of branched chain structure improves the humidity stability of the device [123, 138, 139]. An optimized 2D-3D heterojunction with a large number of high n 2D phases and a small number of remaining PNAI molecules was obtained after a simple interfacial heat treatment process. (n ≥3, n is the number of inorganic layers) A small number of remaining PNAI molecules of 2D-3D heterojunctions. The optimized 2D-3D perovskite heterojunction composition can significantly improve the charge transfer performance, further inhibit interfacial ion defects, increase the Fermi level splitting, reduce the energy bandgap voltage loss (0.38), and finally the open circuit voltage reaches 1.16V (Fig. 11b).

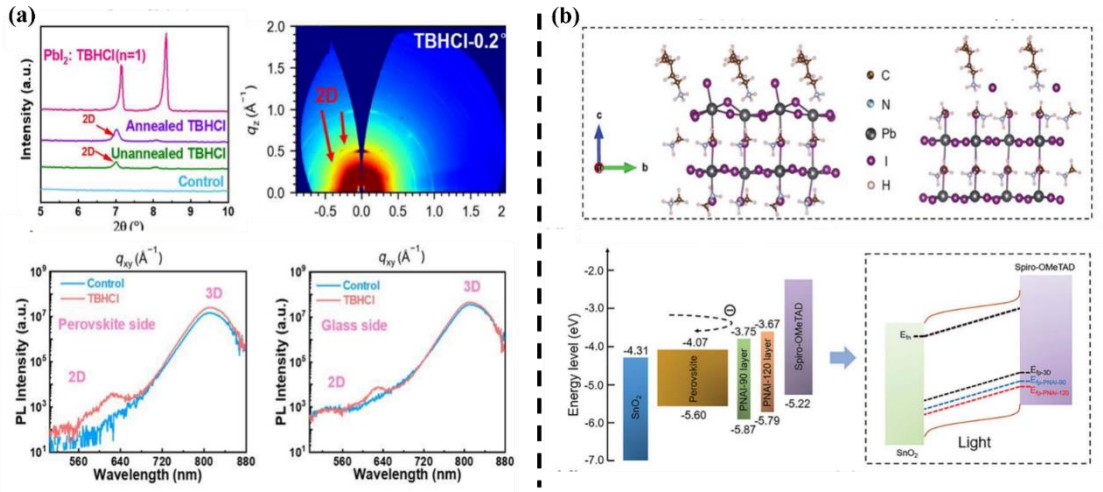

Fig. 11 a SSPL spectra and XRD patterns of unmodified and TBHCl-modified perovskite films and GIWAXS images [136]; **b** DFT calculation of the surface energy of PNAI-treated perovskite, energy level diagram of PSCs and schematic illustration of the Fermi level splitting under light illumination [137]

For 2D/3D perovskite solar cells, in the heterojunction interface, defects and electronic structure determine the energy level arrangement and non-radiative recombination loss [140, 141]. 2D/3D heterojunction can not only improve optical performance, but most of them have passivated defects and improved device quality, but passivation defects are innumerable materials, we will list some of them in the Table 1.

Table 1. Physical properties ad photovoltaic performance of 2D/3D heterojunction based PSC reported in the literature.

2D perovskite	3D perovskite	Band (eV)	Method	V_{OC} (V)	J_{SC} (mA cm^2)	FF	PCE (%)	Stability	Ref
CF_3PEAI	$(FAPbI_3)_{1-x}(MAPbBr_{3-y}Cl_y)_x$	-	Post treatment	1.11	24.25	78.21	21.05	98% of initial PCE, 528h, RH 70-80%	[142]
PEABr	$(FA_{0.6}MA_{0.4})PbI_3$	-	Post treatment (dissolved in IPA）	1.105	23.95	79	20.57	>90% of initial PCE after a monthRT, 91% of initial PCE,100 days, drying oven,dark	[143]
BA	$MAPbI_3$	-	Post treatment	1.11	22.49	78	19.56	96.5% of initial PCE, 100 h, continuous heating at 95℃	[38]

XDAI	NH_4SCN added $MAPbI_3$	1.61	Post treatment	1.134	23.78	76.92	20.74	80% of initial PCE,1000 h, RH 60%	[144]
2(methyl thiothiol)-4, 5-dihydro1h-imidazole ($MTIm^+$) heterocyclic spacer cation	$(Cs_{0.05}FA_{0.95}PbI_3)_{0.85}(MAPbBr_3)_{0.15}$	1.62	Dissolved in perovskite precursor	1.14	23.56	79.12	21.25	94% of initial PCE, 2880h,RH 50%	[145]
4,4′-bipiperidine (BiPi)-based organic salt，$BiPiI_2$	$CH_3NH_3PbI_3$	1.58	Two step method （dissolved in IPA）	1.10	23.51	77	20.03	95% of initial PCE,1000h ,RH ca. 30%	[146]
2-PyEAI	$FA_{0.92}MA_{0.08}PbI_3$	1.55	Post treatment (dissolved in IPA)	1.14	24.8	82.1	23.2	92% of initial PCE, 3000 h, RH 30%	[87]
(Gly-X: X = Cl, Br, and **I**)	$CsPbI_2Br$	1.91	spin-coating method	1.33	16.04	80.92	17.26	96.6% of initial PCE, 50 days,≈30 ℃,RH30%	[147]
GuX(X = Cl, Br, and **I**)	$FAPbI_3$	1.51	GuCl integral doping and GuI surface post-treatment	1.12	24.79	81.15	22.53	>90% of initial PCE, 30day, RH 20%	[148]
β-GUA	$FA_{0.95}Cs_{0.05}PbI_3$	1.52	spin-coating method	1.14	24.41	79.6	22.2	-	[128]
$(NpMA)_2PbI_4$	$FA_{0.85}MA_{0.15}PbI_3$	1.55	Two step method	1.18	25.30	81.36	24.37	85.8% of initial PCE, 2158h RH,30±5%	[149]
1,8-naphthyridine (1,8-ND)	$(FA_{0.92}MA_{0.08}PbI_3$	1.55	Post treatment	1.15	24.9	83.0	23.8	83.2% of initial PCE, 50	[113]

								days, RH 30%	
OLAI(Invert)	$Cs_{0.07}FA_{0.93}PbI_3$	1.55	Post treatment	1.20	24.69	82	24.3	>95% of the initial PCE (T95),1 2 0 0 h, damp-heat test of encapsulated	[150]
DABr	$FA_{0.9}MA_{0.1}PbI_3$	-	Post treatment	1.11	25.14	0.78	21.81	64% of the initial PCE,1065h ,15% RH in air	[130]
Multifunctional TiO_2 Nanoparticles (NPs) Modified Carbon Nanotubes (CNT:TiO_2)	$Cs_{0.05}(MA_{0.15}FA_{0.85})_{0.95}Pb(I_{0.85}Br_{0.15})_3$	-	Dissolved in perovskite precursor	1.2	24.85	0.76	22.7	91% of the initial PCE, 744 h, RH 20-40%	[151]
Linear alkyl ammonium bromide/chloroform (C6Br/CF)	$(FAPbI_3)_{0.92}(MAPbBr_3)_{0.08}$	1.56	Post treatment	1.16	24.5	82.3	23.4	85% of the initial PCE, MPPT, 500h	[125]
A-PPG	$Cs_{0.05}(MA_{0.17}FA_{0.83})_{0.95}Pb(I_{0.83}Br_{0.17})_3$	1.61	Post treatment	1.21	23.27	78.97	22.24	90% of the initial PCE, 50days, RH 30±10%	[152]
PNAI	$(CsPbI_3)_x(FAPbI_3)_y(MAPbBr_3)_{1-x-y}$	1.53-1.54	Post treatment (dissolved in IPA)	1.16	23.82	81.87	22.62	89% of the initial PCE, 1000 h, RH 30±5%	[137]
PMAI	$Cs_{0.05}(MA_{0.17}FA_{0.83})_{0.95}Pb(I_{0.83}Br_{0.17})_3$	-	Post treatment (dissolved in IPA)	1.174	23.07	73.92	20.02	93.02% of the initial PCE, 720 hours,	[153]

								drying tower at RT	
TEACl	$FA_{0.8}Cs_{0.2}Pb(I_{0.8}Br_{0.2})_3$	1.68		1.19	20.94	81.8	20.31	92.8% of the initial PCE, 315 h, RH 40%	[133]
TBHCl	$Rb_{0.02(}FA_{0.95}C_{s0.05})_{0.98}PbI_{2.91}Br_{0.03}Cl_{0.06}$	1.54	Post treatment (dissolved in IPA)	1.186	22.60	0.841	22.54	89% of the initial PCE, 1656 h,RH 10−20%	[136]
4-hydroxy-phenylethylamine iodide (OH-PEAI)	$Rb_{0.05}Cs_{0.05}[(FA_{0.83}MA_{0.17})]_{0.9}Pb(I_{0.83}Br_{0.17})_3$	1.61	Post treatment (disslovede in IPA)	1.22	23.25	75.50	21.38	93% of the initial PCE, unencapsulated 48h, RH 30%	[131]
D-4-tert-butylphenylalanine (D4TBP)	$Cs_{0.05}FA_{0.81}MA_{0.14}PbI_{2.55}Br_{0.45}$(Invert)	1.57	Post treatment (disslovede in IPA)）	1.21	22.49	0.785	21.4	-	[154]
1-naphthylmethylamine(NMA)	$MAPbI_3$	-	Dissolved in perovskite precursor	1.16	21.7	0.80	20.1	-	[155]
(2-CF_3-PEAI)	$FAPbI_3$	-	Post treatment (disslovede in IPA)	1.14	24.4	83.0	23.17	81% of the initial PCE,RT under continuous illumination in the presence of N2 850h	[156]
GUA_2PbI_4	$Cs_{0.3}FA_{0.6}DMA_{0.1}PbI_{2.4}Br_{0.6}$ (Invert)	1.70	Dissolved in perovskite precursor	1.23	20.1	81.6	20.1	>90% of the initial PCE, 30 days, dark glovebox	[141]
	$Cs_{0.05}FA_{0.85}MA_{0.1}PbI_3$	1.55		1.17	24.1	81.6	22.9	-	

3.4 Carrier dynamics

Since people have been chasing the stability of 3D perovskites, they began to combine 2D/3D perovskites, but this leads to some changes in photoelectric properties, which would sacrifice a certain amount of absorbing light, thereby reducing carrier mobility and diffusion length, so as to better understand the trend of photoelectric characteristics, clarify the influence of electronic constraints on photoelectric performance, and help to better understand how to adjust these 2D/3D hybrid materials and optimize devices [127, 157, 158].

Chen et al. [159] reported a high performance photoelectric perovskite based on $PEA_2PbI_4/MAPbI_3$ bilayer after steam annealing of 1-butanol. Compared with 3D $MAPbI_3$ film, $PEA_2PbI_4/MAPbI_3$ bilayer film annealed based on 1-butanol vapor has higher embedded potential, inhibited carrier recombination, increased charge transport, and shortened carrier extraction time. At room temperature, the perovskite photodetectors of $PEA_2PbI_4/MAPbI_3$ bilayers after gas phase annealing are significantly reduced, the photoresponse rate is 1.38 AW^{-1}, the detection rate is 6.52 × 1014 Jones (1 Jones = 1 cm $HZ^{1/2}$ W^{-1}), and the linear dynamic range is more than 167dB. These results demonstrated that a simple method to approach high-performance perovskite photovoltaics has been developed. Lin et al. [155] added a low concentration of the large cation 1-naphthalene methylamine (NMA) to p-i-n perovskite solar cells (PSCs) in a simple way to maximize V_{OC} and provided insights into the large cation-induced morphological control and carrier dynamics of PSCs.As more NMA is added during processing, the PL intensity increases, the non-radiative recombination is

inhibited, and the loss of PL quenching efficiency (PLQE) at high NMA concentrations indicates that charge transfer to the electron transport layer is obstructed (Fig. 12a). Using time-dependent single-photon counting (TCSPC), the trend of steady-state PL intensity with NMA concentration and charge transport layer addition was observed. Transient PL data with a charge transport layer indicate that high NMA concentrations prevent the efficient transfer of free carriers to the charge transport layer. Finally, the amplitude plots of NMA % (red) and the slowest attenuation phase (A3, blue) of the device Jsc of PTAA/perovskite/PCBM thin film show that the amplitude increase is related to the loss of J_{SC}, which explains why larger organic cationic additives can only enhance the performance of PSCs at lower additive concentrations, and this limitation may be beneficial to the application of light-emitting diodes (LEDs) (Fig. 12b).

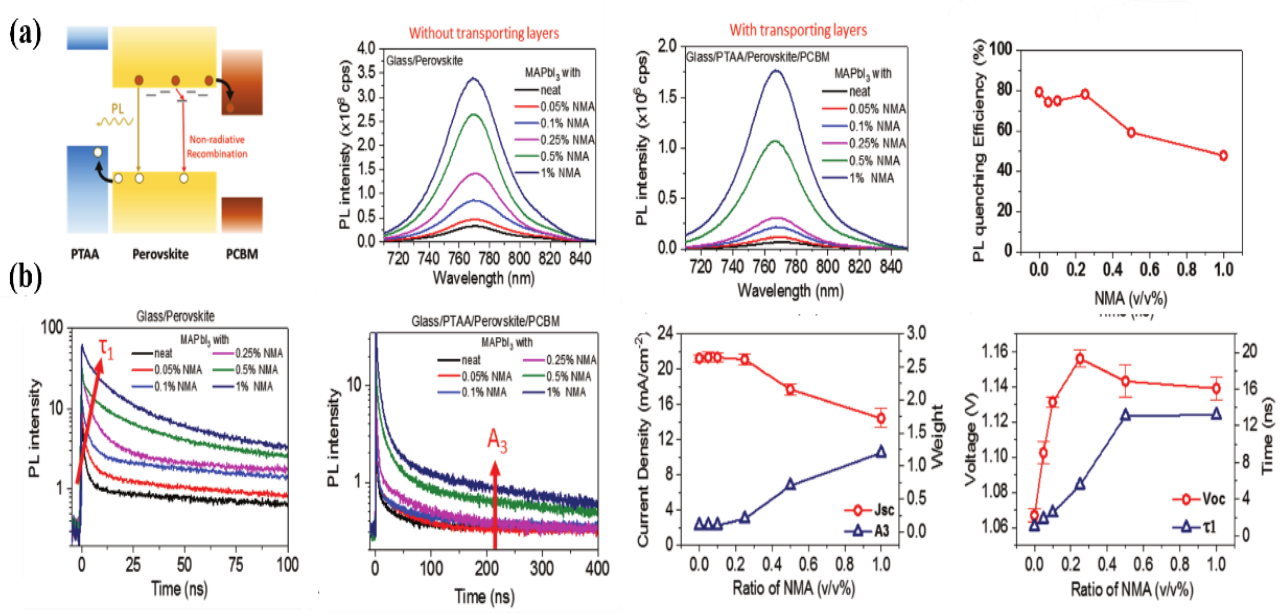

Fig. 12 a Charge transfer path and PL spectra corresponding to $MAPbI_3$, PTAA and PCBM transport layer sandwich membranes at NMA of 0.05 ~ 1 vol% to determine the PL quenching efficiency (PLQE) generated by the charge transfer layer. **b** Time-dependent single-photon counting (TCSPC)

765 on bare and charge transport layers interface membranes after NMA addition, as well as fitted J_{SC}
766 amplitude maps and V_{OC} ratio degrees, with higher concentrations of NMA leading to increased
767 inhibition of charge transfer to the transport layer, resulting in J_{SC} loss due to increased bimolecular
768 recombination loss [159]
769
770 Leonardo R. V. Buizza et al. [160] studied the charge carrier dynamics, especially
771 the recombination rate and mobility, of 2D-3D hybrid perovskite $BA_x(FA_{0.83}Cs_{0.17})_{1-x}$
772 $Pb(I_{0.6}Br_{0.4})_3$ system with different BA contents ($0 \leq x \leq 0.8$). It is suggested that a small
773 amount of ammonium butadium (BA) is helpful to increase crystallinity and passivate
774 grain boundaries, thereby reducing the charge-carrier recombination mediated by traps
775 and improving the charge-carrier mobility. Due to the weakened dispersive force
776 associated with the high electronnegativity of fluorine (F), fluoride compounds are
777 usually hydrophobic and hardly soaked by water. Liu et al. [161] introduced a two-
778 dimensional A_2PbI_4 perovskite layer, inserting pentafluorophenyl ammonium (FEA) as
779 a fluoroaromatic cation between a three-dimensional light-trapping perovskite film and
780 a hole transport material (HTM). The perfluorobenzene unit was introduced to shape
781 the electronic characteristics of the aromatic core, promote hole extraction and inhibit
782 interlayer ion migration at the same time, so as to prepare efficient bilayer 3D/2D PSCs
783 with excellent water stability. This is a kind of superhydrophobic 2D perovskite
784 material. The 2D layer also enhances the extraction of boundary faces and inhibits non-
785 radiative carrier recombination. The power conversion efficiency (PCE) reaches 22%.
786 Shen et al. [31] reported the mixing of new 2D perovskites with 3D perovskites,
787 Nd^{3+} replaced part of the Pb^{2+} in the PEA_2PbI_4:$MAPbI_3$ perovskite film, obtained a
788 higher quality film, promoted and balanced charge transport. Total internal reflection
789 fluorescence microscopy (TIRFM) was used to study the PL intensity map of perovskite

790 particles (Fig. 13a). The introduction of Nd^{3+} leads to a significant increase in the
791 photoluminescence (PL) intensity of the perovskite, and the non-radiative complexation
792 within the chalcogenide is suppressed. The transient absorption kinetics and the
793 transient absorption spectra (TAS) of perovskite thin films are shown in Fig. 13b, the
794 longer lifetimes obtained after the modification are demonstrated by fitting the kinetics.
795 These are attributed to fewer defects, higher crystallinity, and larger grain size of the
796 perovskite films, thus exhibiting higher J_{SC}, in agreement with the previously described
797 results. Li et al. [162] incorporated alternating spacer cations 4-(aminoethyl) pyridine
798 (4-AEP) and phenylethylamine (PEA) into MA-based perovskites and prepared
799 perovskite films using a one-step spin-coating method to compare the effects on the
800 performance of the corresponding PSCs. The results showed that $MAPbI_3$(2D/3D)
801 PSCs incorporating 4-AEP obtained higher PCE. Based on ITO /SnO_2/
802 perovskite/PCBM/Ag pure electronic structures were subjected to space charge limited
803 current (SCLC) measurements for quantitative analysis of the trap density of states (Fig.
804 13c). The lowest value of trap state density (N_t) was calculated for 4-AEP spacer cation
805 based films according to the equation $N_t = 2\varepsilon_0\varepsilon_r/(qL^2)$, where ε_0 is the vacuum
806 permittivity, ε_r is the relative dielectric constant of the $MAPbI_3$ perovskite, q is the
807 elemental charge and L represents the film thickness. This indicates an effective
808 passivation of the perovskite defects by organic spacer cations with reduced V_{OC} loss.
809 The dependence of V_{OC} on light intensity was used to evaluate the carrier complexation
810 mechanism in the PSC **(**Fig. 13d**)**. The ideal factors of control devices, PEAI and 4-
811 AEPI based devices were 2.46, 1.61 and 1.34 $\kappa T/q$, respectively, and trap-assisted

charge complexation was effectively suppressed, in agreement with the SCLC results. Li et al.[87] introduced 2-(2-pyridyl)ethylamine (2-PyEA) molecules with a two-dimensional structure and a single electron pair of N atoms as a post-treatment modifier onto the perovskite, which promoted the formation of 2D@3D/2D perovskites. The built-in potential (V_{bi}) of the PSCs was analyzed by Mott- Schottky curves (Fig. 13e), and the V_{bi} value increased after optimization of the perovskite by using 2-PyEAI. The increased V_{bi} could strongly drives the separation of photogenerated carriers. The transient photovoltage (TPV) measurements confirm that 2-PyEAI influences the carrier lifetime (Fig. 13f), and a higher decay time of 226 ns was observed for 2D@3D/2D PSCs compared to 3D PSCs (104 ns). All of this demonstrates that the defect density and carrier non-radiative complexation can effectively be suppressed by theoptimization of 2-PyEAI.

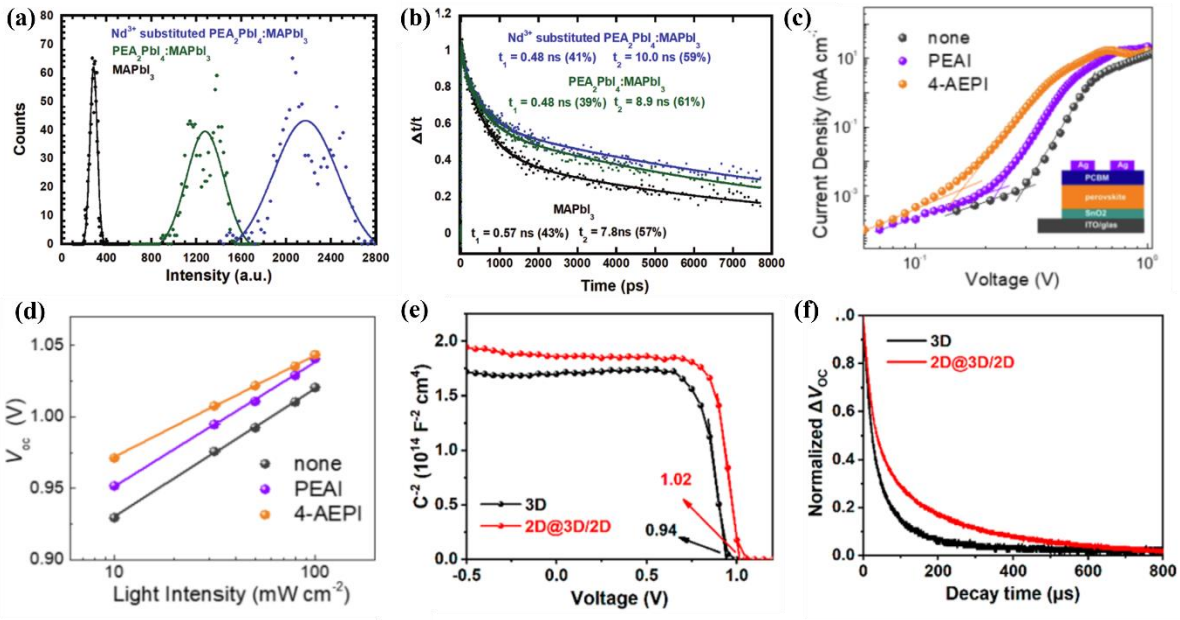

Fig. 13. a, b PL intensity and transient absorption spectra before and after Nd^{3+} substitution [31]; **c,d** SCLC curves and the influence of PEAI or 4-AEPI on V_{OC} [162]; **e** Mott–Schottky plots and **f**

transient photovoltage decay curves as function of 2-PyEA [87]

3.5 Light emitting diode (LED) device

In addition to those mentioned above, three-dimensional (3D) Metal halide perovskites exhibit high emission efficiency, high absorption coefficients, and defect tolerance, however, high excitation fluxes are required to obtain high photoluminescence quantum yields (PLQY) and bright emission. In contrast, low-dimensional perovskites are excellent materials for emission because their quantum well structure can be an ideal platform for exciton generation and, in some cases, self-trapping excitons (STEs) [163, 164]. Due to its own specificity as an excellent optoelectronic material, two-dimensional hetero-metal halide perovskite is a potential host for Rashba/Dresselhaus spin splitting for spin-selective transport and spin orbitals [165]. Due to the unique structural and physical properties it presents, including soft and kinetic structures [166], strong anisotropy [50, 167], room temperature strongly bound excitons [68, 168], Rashba cleavage [165], chirality [169, 170], and ferroelectricity [96, 102, 171], increasing the scope of applications of two-dimensional perovskites in optoelectronics, optoelectronics, and spintronics, two-dimensional (2D)Ruddlesden-Popper perovskites become promising candidates for environmentally stable solar cells, high-efficiency light-emitting diodes and resistive memory devices [172]. Therefore, the ability to combine the properties of both perovskites to complement each other can also lead to unexpected results.

Li et al. [173] introduced ethylenediammonium dibromide ($EDABr_2$) with a molar ratio of 20% in the perovskite precursor solution, and passivated the three-

dimensional perovskite emitter with diammonium molecules without simultaneously producing multiple quantum well (MQW) structures, thereby preparing efficient and stable red PeLEDs. Combined with X-ray photoelectron spectroscopy (XPS) analysis and density functional theory (DFT) calculations, the amorphous quasi-two-dimensional phase rich in EDA-Br forms a cover layer on the surface of the three-dimensional perovskite grain, thereby passivating defects, inhibiting ion of ion migration, and reducing lattice strain (Fig. 14a-f). The optimized device has a peak external quantum efficiency (EQE) of 17.03% at 671 nm, a recorded brightness of 10 745 cd m^{-2}, and an FWHM of 28 nm. A half-life of 15.4 h was obtained, which is the longest half-life of red-emitted 3D PeLEDs. This allows the formation of EDA-Br-rich perovskite cap layers around the three-dimensional perovskite grain surface. There is still a lot to discuss about LED devices, and we will not focus on them here as this review mainly focuses on PSC.

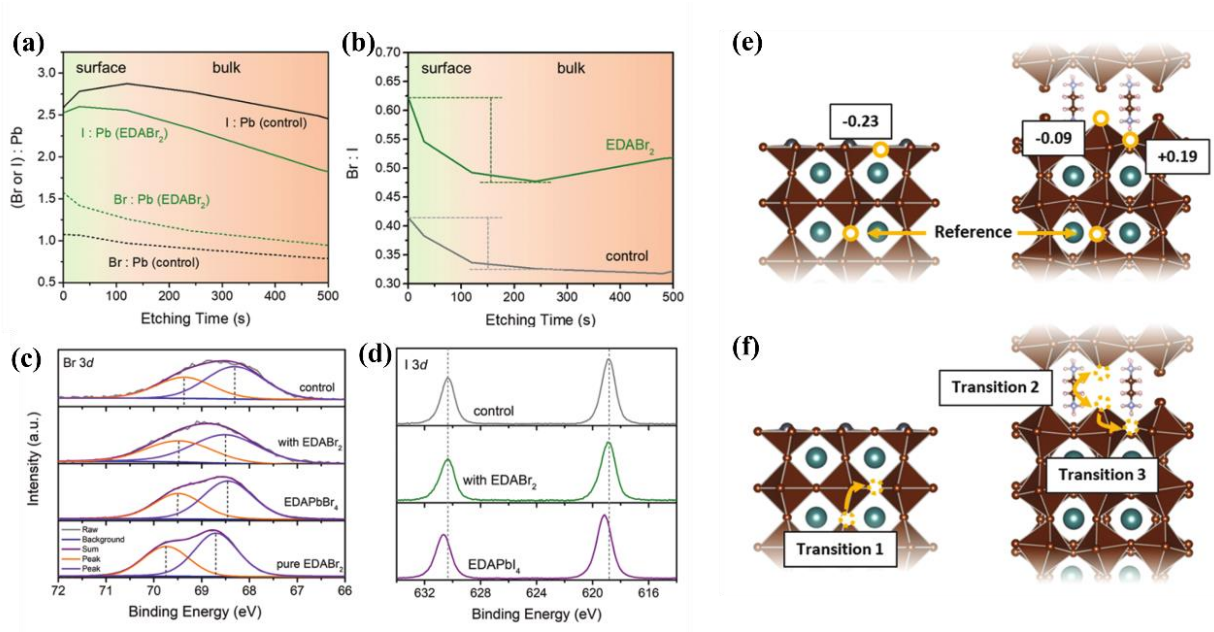

Fig. 14 a-d XPS comparison of different elements. e Br vacancy formation energies on the $CsPbBr_3$ surface and at the $PbBr_6$-EDA interface. f Diffusion paths for Br vacancies in $CsPbBr_3$ (Transition 1) and $EDACs_3Pb_4Br_{13}$ (Transition 2 and 3) [173]

4. Conclusions and Prospects

The review presented an overview of the structure of 2D/3D perovskite and discusses recent research findings, such as surface defect passivation and photovoltaic performance regulation. Also, ideas for synergistically combining 2D and 3D perovskite and providing detailed organization of the passivation effect of 2D materials to facilitate further research were proposed. The goal is the transition of perovskite technology from the research to the commercial space.

The 2D/3D perovskite modified by 2D materials is also developing and progressing, although its efficiency is still far from that of 3D perovskite, and it has been improved considerably in terms of efficiency and stability. The addition of two-dimensional materials not only forms a heterojunction, but also helps to control the growth orientation, selective growth, and improve the crystallinity, while the regulation of the energy band arrangement is more conducive to the extraction of cavities and enhance the efficiency of solar cells. With a wide variety of processes to prepare devices, a wide range of materials to passivate defects, and even a significant increase in hydrophobicity in many devices, the quest to create devices with better performance has been ongoing, and thus closer to commercialization.

Despite the excellent stability of two-dimensional perovskite, however, efficiency remains a major issue, even though the great breakthroughs in recent years. Its potential for light-emitting devices is unlimited, and among the various photophysical properties,

890 the nature of the excited state species plays a decisive role in the dynamics and
891 properties of the excited state, which is the core of semiconductor photophysics
892 research [174], and this property is also an inspiration for our exploration of perovskite
893 solar cells. If the higher exciton binding energies and anisotropic charge transport
894 properties of excited state dynamics in two-dimensional perovskites are applied to
895 three-dimensional perovskites, and if tests methods are found to provide a deeper and
896 more comprehensive explanation of these fundamental theories, it will be a further step
897 forward in terms of how to adjust the crystal orientation, or to make the results of our
898 work more convincing by using the interpretation of carrier dynamics. This would be
899 an even greater step forward in terms of how to adjust the crystal orientation, or use
900 carrier dynamics to make the results of our work more convincing.In addition to some
901 testing methods, we have also developed a variety of approaches to prepare devices,
902 including the common one-step spin-coating method, two-step method, solution
903 processing techniques, as well as thermal casting-assisted solution methods, low-
904 pressure steam-assisted solution processes, and precursor dissolution (SPD) strategies
905 [125], Researchers have continued to explore and optimize them in the hope of making
906 breakthroughs in efficiency. In a recent study, the team of A.D Mohite and Jackey Even
907 from Rice University, Sidhik et al. [41] reported a method to prepare 2D/3D perovskite
908 heterojunctions by dissolution engineering with an efficiency of 24.5%, thus it seems
909 that there is still a great potential for 2D/3D perovskite solar cells. The potential of
910 2D/3D perovskite solar cells is still very large, and there is still a lot of potential to be
911 explored to innovate and find the appropriate preparation method or to synthesize the

material properties for better integration of materials and techniques to maximize the benefits. Finally, there is a wide range of 2D materials used to modify 3D perovskites, and most of them play the role of passivation defects, and the types are similar in a comprehensive view. Whether we can discover or create different modification materials is what we will continue to explore in the future, and not be bound by the current results to create more value, the search for new perovskites with excellent inherent stability has become an inevitable way to meet the stability requirements of commercial operation [145]. In general, there are many challenges facing perovskite solar cells, and many problems have not yet been solved. The joint efforts of researchers are needed to discover the truth behind the experimental phenomenon that is closer to the essence of things. 2D/3D perovskite solar cells will be successfully commercialized in the market as soon as possible.

Funding Information

This work was supported by the China Postdoctoral Science Foundation (2021M690907) and the Natural Science Foundation of Henan Province (No. 202300410073).

Conflicts of interest

Authors declares no conflict of interest.

Author Contribution

Xiaohui Li: conceptualization, writing-original draft, Putao Zhang: conceptualization, project administration, writing-review, and editing; Shengjun Li: conceptualization, writing-review, and editing, Priyanka Wasnik: writing-original draft; Junna Ren: writing-original draft; Qinglong Jiang; writing-review and editing; Ben Bin Xu: writing-review and editing and Vignesh Murugadoss: conceptualization, writing-review,

and editing.

References

1. Kojima A, Teshima K, Shirai Y, and Miyasaka T (2009) Organometal Halide Perovskites as Visible-Light Sensitizers for Photovoltaic Cells. *Journal of the American Chemical Society* 131(17):6050-6051. http://10.1021/ja809598r
2. <best-research-cell-efficiencies-rev220630-25.7%.pdf>.
3. Chen Y, Wu S, Li X, Liu M, Chen Z, Zhang P, and Li S (2022) Efficient and stable low-cost perovskite solar cells enabled by using surface passivated carbon as the counter electrode. *Journal of Materials Chemistry C* 10(4):1270-1275. http://10.1039/d1tc05351e
4. Zhang P, Chen Y, Wu S, Li X, Liu M, and Li S (2021) Enhancing the performance of n-i-p perovskite solar cells by introducing hydroxyethylpiperazine ethane sulfonic acid for interfacial adjustment. *Nanoscale* 14(1):35-41. http://10.1039/d1nr05939d
5. Xu Z, Zhou X, Li X, and Zhang P (2022) Polymer-Regulated SnO_2 Composites Electron Transport Layer for High-Efficiency n–i–p Perovskite Solar Cells. *Solar RRL* 6(8). http://10.1002/solr.202200092
6. Jeong J, Kim M, Seo J, Lu H, Ahlawat P, Mishra A, Yang Y, Hope M A, Eickemeyer F T, Kim M, Yoon Y J, Choi I W, Darwich B P, Choi S J, Jo Y, Lee J H, Walker B, Zakeeruddin S M, Emsley L, Rothlisberger U, Hagfeldt A, Kim D S, Gratzel M, and Kim J Y (2021) Pseudo-halide anion engineering for alpha-$FAPbI_3$ perovskite solar cells. *Nature* 592(7854):381-385. http://10.1038/s41586-021-03406-5
7. Yoo J J, Seo G, Chua M R, Park T G, Lu Y, Rotermund F, Kim Y K, Moon C S, Jeon N J, Correa-Baena J P, Bulovic V, Shin S S, Bawendi M G, and Seo J (2021) Efficient perovskite solar cells via improved carrier management. *Nature* 590(7847):587-593. http://10.1038/s41586-021-03285-w
8. Wang P, Chen B, Li R, Wang S, Li Y, Du X, Zhao Y, and Zhang X (2022) 2D perovskite or organic material matter? Targeted growth for efficient perovskite solar cells with efficiency exceeding 24%. *Nano Energy* 94. http://10.1016/j.nanoen.2021.106914
9. Chen J, Yang Y, Dong H, Li J, Zhu X, Xu J, Pan F, Yuan F, Dai J, Jiao B, Hou X, Jen A K Y, and Wu Z Highly efficient and stable perovskite solar cells enabled by low-dimensional perovskitoids. *Science Advances* 8(4):eabk2722. http://10.1126/sciadv.abk2722
10. Kim J H, Kim Y R, Kim J, Oh C M, Hwang I W, Kim J, Zeiske S, Ki T, Kwon S, Kim H, Armin A, Suh H, and Lee K (2022) Efficient and stable perovskite solar cells with a high open-circuit voltage over 1.2 V achieved by a dual-side passivation layer. *Adv Mater*:e2205268. http://10.1002/adma.202205268
11. Li X, Wu S, Chen Y, Tang J, Liu M, Chen Z, Zhang P, and Li S (2022) Grain Boundary Defect Controlling of Perovskite via N-Hydroxysuccinimide Post-Treatment Process in Efficient and Stable n–i–p Perovskite Solar Cells. *Solar RRL* 6(9). http://10.1002/solr.202200502

12. Xu Z, Zhou X, Li X, Li H, Algadi H, and Zhang P (2023) Buried-in interface with two-terminal functional groups for perovskite-based photovoltaic solar cells. *Advanced Composites and Hybrid Materials* 6(2):66. http://10.1007/s42114-023-00646-z
13. Li X, Cuthriell S A, Bergonzoni A, Dong H, Traoré B, Stoumpos C C, Guo P, Even J, Katan C, Schaller R D, and Kanatzidis M G (2022) Expanding the Cage of 2D Bromide Perovskites by Large A-Site Cations. *Chemistry of Materials* 34(3):1132-1142. http://10.1021/acs.chemmater.1c03605
14. Tsai H (2022) The challenges and promises of layered 2D perovskites. *Chem* 8(4):890-891. http://10.1016/j.chempr.2022.03.021
15. Jeon N J, Noh J H, Kim Y C, Yang W S, Ryu S, and Seok S I (2014) Solvent engineering for high-performance inorganic-organic hybrid perovskite solar cells. *Nat Mater* 13(9):897-903. http://10.1038/nmat4014
16. Li Y, Liang C, Wang G, Li J, Chen S, Yang S, Xing G, and Pan H (2020) Two-step solvent post-treatment on PTAA for highly efficient and stable inverted perovskite solar cells. *Photonics Research* 8(10). http://10.1364/prj.398529
17. Cao Y, Liu Z, Li W, Zhao Z, Xiao Z, Lei B, Zi W, Cheng N, Liu J, and Tu Y (2021) Efficient and stable $MAPbI_3$ perovskite solar cells achieved via chlorobenzene/perylene mixed anti-solvent. *Solar Energy* 220:251-257. http://10.1016/j.solener.2021.03.055
18. Shalan A E, Akman E, Sadegh F, and Akin S (2021) Efficient and Stable Perovskite Solar Cells Enabled by Dicarboxylic Acid-Supported Perovskite Crystallization. *J Phys Chem Lett* 12(3):997-1004. http://10.1021/acs.jpclett.0c03566
19. Huang Y, Liu T, Wang B, Li J, Li D, Wang G, Lian Q, Amini A, Chen S, Cheng C, and Xing G (2021) Antisolvent Engineering to Optimize Grain Crystallinity and Hole-Blocking Capability of Perovskite Films for High-Performance Photovoltaics. *Adv Mater* 33(38):e2102816. http://10.1002/adma.202102816
20. Mali S S, Patil J V, Arandiyan H, and Hong C K (2019) Reduced methylammonium triple-cation $Rb_{0.05}(FAPbI_3)_{0.95}(MAPbBr_3)_{0.05}$ perovskite solar cells based on a TiO_2/SnO_2 bilayer electron transport layer approaching a stabilized 21% efficiency: the role of antisolvents. *Journal of Materials Chemistry A* 7(29):17516-17528. http://10.1039/c9ta05422g
21. Kim S G, Kim J H, Ramming P, Zhong Y, Schotz K, Kwon S J, Huettner S, Panzer F, and Park N G (2021) How antisolvent miscibility affects perovskite film wrinkling and photovoltaic properties. *Nat Commun* 12(1):1554. http://10.1038/s41467-021-21803-2
22. Liu C, Huang L, Zhou X, Wang X, Yao J, Liu Z, Liu S F, Ma W, and Xu B (2021) An in-situ defect passivation through a green anti-solvent approach for high-efficiency and stable perovskite solar cells. *Science Bulletin* 66(14):1419-1428. http://10.1016/j.scib.2021.03.018
23. Sun J, Li F, Yuan J, and Ma W (2021) Advances in Metal Halide Perovskite Film Preparation: The Role of Anti-Solvent Treatment. *Small Methods* 5(5). http://10.1002/smtd.202100046
24. Ge S, Zuo S, Zhang M, Luo Y, Yang R, Wu Y, Zhang Y, Li J, and Xia C (2021)

Utilization of decayed wood for polyvinyl chloride/wood flour composites. *Journal of Materials Research and Technology* 12:862-869. http://10.1016/j.jmrt.2021.03.026
25. Liu J, Li N, Jia J, Dong J, Qiu Z, Iqbal S, and Cao B (2019) Perovskite films grown with green mixed anti-solvent for highly efficient solar cells with enhanced stability. *Solar Energy* 181:285-292. http://10.1016/j.solener.2019.02.020
26. Ahmed D S, Mohammed B K, and Mohammed M K A (2021) Long-term stable and hysteresis-free planar perovskite solar cells using green antisolvent strategy. *Journal of Materials Science* 56(27):15205-15214. http://10.1007/s10853-021-06200-w
27. Cao X, Hao L, Liu Z, Su G, He X, Zeng Q, and Wei J (2022) All green solvent engineering of organic–inorganic hybrid perovskite layer for high-performance solar cells. *Chemical Engineering Journal* 437. http://10.1016/j.cej.2022.135458
28. Wang T, Fu Y, Jin L, Deng S, Pan D, Dong L, Jin S, and Huang L (2020) Phenethylammonium Functionalization Enhances Near-Surface Carrier Diffusion in Hybrid Perovskites. *Journal of the American Chemical Society* 142(38):16254-16264. http://10.1021/jacs.0c04377
29. Seitz M, Magdaleno A J, Alcazar-Cano N, Melendez M, Lubbers T J, Walraven S W, Pakdel S, Prada E, Delgado-Buscalioni R, and Prins F (2020) Exciton diffusion in two-dimensional metal-halide perovskites. *Nat Commun* 11(1):2035. http://10.1038/s41467-020-15882-w
30. Chen H, Zhan Y, Xu G, Chen W, Wang S, Zhang M, Li Y, and Li Y (2020) Organic N-Type Molecule: Managing the Electronic States of Bulk Perovskite for High-Performance Photovoltaics. *Advanced Functional Materials* 30(36). http://10.1002/adfm.202001788
31. Shen L, Chen R, Zhang D, Yilmazoglu U C, Gu K, Sarmiento J S, Zhu T, Zheng L, Zheng J, Wang H, Liu C, and Gong X (2022) High-Performance Perovskite Photovoltaics by Heterovalent Substituted Mixed Perovskites. *Advanced Functional Materials*. http://10.1002/adfm.202207911
32. Cao Q, Li P, Chen W, Zang S, Han L, Zhang Y, and Song Y (2022) Two-dimensional perovskites: Impacts of species, components, and properties of organic spacers on solar cells. *Nano Today* 43. http://10.1016/j.nantod.2022.101394
33. Zhang F, and Zhu K (2021) Breakthrough: Phase-Pure 2D Perovskite Films. *Joule* 5(1):14-15. http://10.1016/j.joule.2020.12.006
34. Chen Y, Sun Y, Peng J, Tang J, Zheng K, and Liang Z (2018) 2D Ruddlesden-Popper Perovskites for Optoelectronics. *Adv Mater* 30(2). http://10.1002/adma.201703487
35. Shao M, Bie T, Yang L, Gao Y, Jin X, He F, Zheng N, Yu Y, and Zhang X (2022) Over 21% Efficiency Stable 2D Perovskite Solar Cells. *Adv Mater* 34(1):e2107211. http://10.1002/adma.202107211
36. Wu G, Liang R, Ge M, Sun G, Zhang Y, and Xing G (2022) Surface Passivation Using 2D Perovskites toward Efficient and Stable Perovskite Solar Cells. *Adv Mater* 34(8):e2105635. http://10.1002/adma.202105635
37. Smith I C, Hoke E T, Solis-Ibarra D, McGehee M D, and Karunadasa H I (2014) A Layered Hybrid Perovskite Solar-Cell Absorber with Enhanced Moisture Stability.

Angewandte Chemie International Edition 53(42):11232-11235. http://10.1002/anie.201406466

38. Lin Y, Bai Y, Fang Y, Chen Z, Yang S, Zheng X, Tang S, Liu Y, Zhao J, and Huang J (2018) Enhanced Thermal Stability in Perovskite Solar Cells by Assembling 2D/3D Stacking Structures. *J Phys Chem Lett* 9(3):654-658. http://10.1021/acs.jpclett.7b02679
39. Zheng L, Shen L, Zhu T, Zhang D, Zheng J, and Gong X (2022) Stable and efficient perovskite solar cells by discrete two-dimensional perovskites capped on the three-dimensional perovskites bilayer thin film. *Nano Energy* 96. http://10.1016/j.nanoen.2022.107126
40. Zhang X, Zhou W, Chen X, Chen Y, Li X, Wang M, Zhou Y, Yan H, Zheng Z, and Zhang Y (2022) Dual Optimization of Bulk and Surface via Guanidine Halide for Efficient and Stable 2D/3D Hybrid Perovskite Solar Cells. *Advanced Energy Materials*. http://10.1002/aenm.202201105
41. Sidhik S, Wang Y, De Siena M, Asadpour R, Torma A J, Terlier T, Ho K, Li W, Puthirath A B, Shuai X, Agrawal A, Traore B, Jones M, Giridharagopal R, Ajayan P M, Strzalka J, Ginger D S, Katan C, Alam M A, Even J, Kanatzidis M G, and Mohite A D (2022) Deterministic fabrication of 3D/2D perovskite bilayer stacks for durable and efficient solar cells. *Science* 377(6613):1425-1430. http://10.1126/science.abq7652
42. Mahmud M A, Duong T, Peng J, Wu Y, Shen H, Walter D, Nguyen H T, Mozaffari N, Tabi G D, Catchpole K R, Weber K J, and White T P (2021) Origin of Efficiency and Stability Enhancement in High-Performing Mixed Dimensional 2D-3D Perovskite Solar Cells: A Review. *Advanced Functional Materials* 32(3). http://10.1002/adfm.202009164
43. Krishna A, Gottis S, Nazeeruddin M K, and Sauvage F (2019) Mixed Dimensional 2D/3D Hybrid Perovskite Absorbers: The Future of Perovskite Solar Cells? *Advanced Functional Materials* 29(8). http://10.1002/adfm.201806482
44. He T, Jiang Y, Xing X, and Yuan M (2020) Structured Perovskite Light Absorbers for Efficient and Stable Photovoltaics. *Adv Mater* 32(26):e1903937. http://10.1002/adma.201903937
45. Kim E-B, Akhtar M S, Shin H-S, Ameen S, and Nazeeruddin M K (2021) A review on two-dimensional (2D) and 2D-3D multidimensional perovskite solar cells: Perovskites structures, stability, and photovoltaic performances. *Journal of Photochemistry and Photobiology C: Photochemistry Reviews* 48. http://10.1016/j.jphotochemrev.2021.100405
46. Ge S, Shi Y, Xia C, Huang Z, Manzo M, Cai L, Ma H, Zhang S, Jiang J, Sonne C, and Lam S S (2021) Progress in pyrolysis conversion of waste into value-added liquid pyro-oil, with focus on heating source and machine learning analysis. *Energy Conversion and Management* 245. http://10.1016/j.enconman.2021.114638
47. Sun Y, Zhang L, Wang N, Zhang S, Cao Y, Miao Y, Xu M, Zhang H, Li H, Yi C, Wang J, and Huang W (2018) The formation of perovskite multiple quantum well structures for high performance light-emitting diodes. *npj Flexible Electronics* 2(1). http://10.1038/s41528-018-0026-0

48. Zou W, Li R, Zhang S, Liu Y, Wang N, Cao Y, Miao Y, Xu M, Guo Q, Di D, Zhang L, Yi C, Gao F, Friend R H, Wang J, and Huang W (2018) Minimising efficiency roll-off in high-brightness perovskite light-emitting diodes. *Nat Commun* 9(1):608. http://10.1038/s41467-018-03049-7
49. Saparov B, and Mitzi D B (2016) Organic-Inorganic Perovskites: Structural Versatility for Functional Materials Design. *Chem Rev* 116(7):4558-4596. http://10.1021/acs.chemrev.5b00715
50. Wen X, and Jia B (2022) New insight into carrier transport in 2D layered perovskites. *Chem* 8(4):904-906. http://10.1016/j.chempr.2022.03.014
51. Sirbu D, Balogun F H, Milot R L, and Docampo P (2021) Layered Perovskites in Solar Cells: Structure, Optoelectronic Properties, and Device Design. *Advanced Energy Materials* 11(24). http://10.1002/aenm.202003877
52. Wang H, Zhang X, Ma Y, Wang M, and Wang J (2022) A Universal Approach for Potassium-Passivated 2D Perovskites. *Solar RRL* 6(6). http://10.1002/solr.202101019
53. Jiang T, Min H, Zou R, Wang M, Wen K, Lai J, Xu L, Wang Y, Xu W, Wang C, Wei K, Medhekar N V, Peng Q, Chang J, Huang W, and Wang J (2022) Molecularly Controlled Quantum Well Width Distribution and Optoelectronic Properties in Quasi-2D Perovskite Light-Emitting Diodes. *J Phys Chem Lett* 13(18):4098-4103. http://10.1021/acs.jpclett.2c00360
54. Zhang Y, Li F, Jiang K-J, Huang J-H, Wang H, Fan H, Wang P, Liu C-M, Zhang L-P, and Song Y (2018) From 2D to 3D: a facile and effective procedure for fabrication of planar CH3NH3PbI3perovskite solar cells. *Journal of Materials Chemistry A* 6(37):17867-17873. http://10.1039/c8ta07048b
55. Mahmud M A, Duong T, Yin Y, Pham H T, Walter D, Peng J, Wu Y, Li L, Shen H, Wu N, Mozaffari N, Andersson G, Catchpole K R, Weber K J, and White T P (2019) Double-Sided Surface Passivation of 3D Perovskite Film for High-Efficiency Mixed-Dimensional Perovskite Solar Cells. *Advanced Functional Materials* 30(7). http://10.1002/adfm.201907962
56. Liu C, Fang Z, Sun J, Lou Q, Ge J, Chen X, Zhou E, Shang M-H, Yang W, and Ge Z (2020) Imidazolium Ionic Liquid as Organic Spacer for Tuning the Excitonic Structure of 2D Perovskite Materials. *ACS Energy Letters* 5(11):3617-3627. http://10.1021/acsenergylett.0c01784
57. Niu T, Lu J, Jia X, Xu Z, Tang M C, Barrit D, Yuan N, Ding J, Zhang X, Fan Y, Luo T, Zhang Y, Smilgies D M, Liu Z, Amassian A, Jin S, Zhao K, and Liu S (2019) Interfacial Engineering at the 2D/3D Heterojunction for High-Performance Perovskite Solar Cells. *Nano Lett* 19(10):7181-7190. http://10.1021/acs.nanolett.9b02781
58. Yang F, Zhang P, Kamarudin M A, Kapil G, Ma T, and Hayase S (2018) Addition Effect of Pyrene ammonium Iodide to Methylammonium Lead Halide Perovskite-2D/3D Heterostructured Perovskite with Enhanced Stability. *Advanced Functional Materials* 28(46). http://10.1002/adfm.201804856
59. Ge S, Ma N L, Jiang S, Ok Y S, Lam S S, Li C, Shi S Q, Nie X, Qiu Y, Li D, Wu Q, Tsang D C W, Peng W, and Sonne C (2020) Processed Bamboo as a Novel

Formaldehyde-Free High-Performance Furniture Biocomposite. *ACS Appl Mater Interfaces* 12(27):30824-30832. http://10.1021/acsami.0c07448
60. Zhan Y, Yang F, Chen W, Chen H, Shen Y, Li Y, and Li Y (2021) Elastic Lattice and Excess Charge Carrier Manipulation in 1D-3D Perovskite Solar Cells for Exceptionally Long-Term Operational Stability. *Adv Mater* 33(48):e2105170. http://10.1002/adma.202105170
61. Yang W, Zhan Y, Yang F, and Li Y (2021) Hot-Casting and Anti-solvent Free Fabrication of Efficient and Stable Two-Dimensional Ruddlesden-Popper Perovskite Solar Cells. *ACS Appl Mater Interfaces* 13(51):61039-61046. http://10.1021/acsami.1c17169
62. Zhou T, Lai H, Liu T, Lu D, Wan X, Zhang X, Liu Y, and Chen Y (2019) Highly Efficient and Stable Solar Cells Based on Crystalline Oriented 2D/3D Hybrid Perovskite. *Adv Mater* 31(32):e1901242. http://10.1002/adma.201901242
63. Tang J, Tian W, Zhao C, Sun Q, Zhang C, Cheng H, Shi Y, and Jin S (2022) Imaging the Moisture-Induced Degradation Process of 2D Organolead Halide Perovskites. *ACS Omega* 7(12):10365-10371. http://10.1021/acsomega.1c06989
64. Liang C, Gu H, Xia Y, Wang Z, Liu X, Xia J, Zuo S, Hu Y, Gao X, Hui W, Chao L, Niu T, Fang M, Lu H, Dong H, Yu H, Chen S, Ran X, Song L, Li B, Zhang J, Peng Y, Shao G, Wang J, Chen Y, Xing G, and Huang W (2021) Two-dimensional Ruddlesden–Popper layered perovskite solar cells based on phase-pure thin films. *Nature Energy* 6(1):38-45. http://10.1038/s41560-020-00721-5
65. Mao L, Kennard R M, Traore B, Ke W, Katan C, Even J, Chabinyc M L, Stoumpos C C, and Kanatzidis M G (2019) Seven-Layered 2D Hybrid Lead Iodide Perovskites. *Chem* 5(10):2593-2604. http://10.1016/j.chempr.2019.07.024
66. Kepenekian M, Traore B, Blancon J C, Pedesseau L, Tsai H, Nie W, Stoumpos C C, Kanatzidis M G, Even J, Mohite A D, Tretiak S, and Katan C (2018) Concept of Lattice Mismatch and Emergence of Surface States in Two-dimensional Hybrid Perovskite Quantum Wells. *Nano Lett* 18(9):5603-5609. http://10.1021/acs.nanolett.8b02078
67. Yu S, Meng J, Pan Q, Zhao Q, Pullerits T, Yang Y, Zheng K, and Liang Z (2022) Imidazole additives in 2D halide perovskites: impacts of –CN versus –CH_3 substituents reveal the mediation of crystal growth by phase buffering. *Energy & Environmental Science* 15(8):3321-3330. http://10.1039/d2ee00571a
68. Dyksik M, Duim H, Maude D K, Baranowski M, Loi M A, and Plochocka P Brightening of dark excitons in 2D perovskites. *Science Advances* 7(46):eabk0904. http://10.1126/sciadv.abk0904
69. Xu Y, Wang M, Lei Y, Ci Z, and Jin Z (2020) Crystallization Kinetics in 2D Perovskite Solar Cells. *Advanced Energy Materials* 10(43). http://10.1002/aenm.202002558
70. Ramakrishnan S, Li H, Xu Y, Shin D, Dursun I, Cotlet M, Zhang Y, and Yu Q (2022) Ruddlesden–Popper Perovskites with Narrow Phase Distribution for Air-Stable Solar Cells. *Solar RRL* 6(9). http://10.1002/solr.202200490
71. Caiazzo A, and Janssen R A J (2022) High Efficiency Quasi-2D Ruddlesden–Popper Perovskite Solar Cells. *Advanced Energy Materials*.

http://10.1002/aenm.202202830
72. Li X, Hoffman J M, and Kanatzidis M G (2021) The 2D Halide Perovskite Rulebook: How the Spacer Influences Everything from the Structure to Optoelectronic Device Efficiency. *Chem Rev* 121(4):2230-2291. http://10.1021/acs.chemrev.0c01006
73. Zheng Y, Chen S-C, Ma Y, and Zheng Q (2022) Furfurylammonium as a Spacer for Efficient 2D Ruddlesden–Popper Perovskite Solar Cells. *Solar RRL* 6(8). http://10.1002/solr.202200221
74. Wang Y R, Senocrate A, Mladenović M, Dučinskas A, Kim G Y, Rothlisberger U, Milić J V, Moia D, Grätzel M, and Maier J (2022) Photo De-Mixing in Dion-Jacobson 2D Mixed Halide Perovskites. *Advanced Energy Materials* 12(26). http://10.1002/aenm.202200768
75. Mao L, Ke W, Pedesseau L, Wu Y, Katan C, Even J, Wasielewski M R, Stoumpos C C, and Kanatzidis M G (2018) Hybrid Dion-Jacobson 2D Lead Iodide Perovskites. *J Am Chem Soc* 140(10):3775-3783. http://10.1021/jacs.8b00542
76. Zeng Z, Chen X, Yue Y, Li S, Chai N, Mai B, Meng J, Cheng Y-B, and Wang X (2022) Photo-Induced Degradation of 2D Dion−Jacobson Perovskites under Continuous Light Illumination. *Solar RRL*. http://10.1002/solr.202200359
77. Xu Z, Lu D, Dong X, Chen M, Fu Q, and Liu Y (2021) Highly Efficient and Stable Dion-Jacobson Perovskite Solar Cells Enabled by Extended pi-Conjugation of Organic Spacer. *Adv Mater* 33(51):e2105083. http://10.1002/adma.202105083
78. Fu H (2021) Dion–Jacobson halide perovskites for photovoltaic and photodetection applications. *Journal of Materials Chemistry C* 9(20):6378-6394. http://10.1039/d1tc01061a
79. Ke W, Mao L, Stoumpos C C, Hoffman J, Spanopoulos I, Mohite A D, and Kanatzidis M G (2019) Compositional and Solvent Engineering in Dion–Jacobson 2D Perovskites Boosts Solar Cell Efficiency and Stability. *Advanced Energy Materials* 9(10). http://10.1002/aenm.201803384
80. Ahmad S, Fu P, Yu S, Yang Q, Liu X, Wang X, Wang X, Guo X, and Li C (2019) Dion-Jacobson Phase 2D Layered Perovskites for Solar Cells with Ultrahigh Stability. *Joule* 3(3):794-806. http://10.1016/j.joule.2018.11.026
81. Huang P, Kazim S, Wang M, and Ahmad S (2019) Toward Phase Stability: Dion–Jacobson Layered Perovskite for Solar Cells. *ACS Energy Letters* 4(12):2960-2974. http://10.1021/acsenergylett.9b02063
82. Zhang F, Lu H, Tong J, Berry J J, Beard M C, and Zhu K (2020) Advances in two-dimensional organic–inorganic hybrid perovskites. *Energy & Environmental Science* 13(4):1154-1186. http://10.1039/c9ee03757h
83. Mao L, Stoumpos C C, and Kanatzidis M G (2019) Two-Dimensional Hybrid Halide Perovskites: Principles and Promises. *J Am Chem Soc* 141(3):1171-1190. http://10.1021/jacs.8b10851
84. Ma C, Shen D, Ng T W, Lo M F, and Lee C S (2018) 2D Perovskites with Short Interlayer Distance for High-Performance Solar Cell Application. *Adv Mater* 30(22):e1800710. http://10.1002/adma.201800710
85. Cohen B E, Li Y, Meng Q, and Etgar L (2019) Dion-Jacobson Two-Dimensional

Perovskite Solar Cells Based on Benzene Dimethanammonium Cation. *Nano Lett* 19(4):2588-2597. http://10.1021/acs.nanolett.9b00387
86. Lin Y-H, Sakai N, Da P, Wu J, Sansom H C, Ramadan A J, Mahesh S, Liu J, Oliver R D J, Lim J, Aspitarte L, Sharma K, Madhu P K, Morales-Vilches A B, Nayak P K, Bai S, Gao F, Grovenor C R M, Johnston M B, Labram J G, Durrant J R, Ball J M, Wenger B, Stannowski B, and Snaith H J (2020) A piperidinium salt stabilizes efficient metal-halide perovskite solar cells. *Science* 369(6499):96-102. http://doi:10.1126/science.aba1628
87. Li G, Song J, Wu J, Song Z, Wang X, Sun W, Fan L, Lin J, Huang M, Lan Z, and Gao P (2021) Efficient and Stable 2D@3D/2D Perovskite Solar Cells Based on Dual Optimization of Grain Boundary and Interface. *ACS Energy Letters* 6(10):3614-3623. http://10.1021/acsenergylett.1c01649
88. Lu D, Lv G, Xu Z, Dong Y, Ji X, and Liu Y (2020) Thiophene-Based Two-Dimensional Dion-Jacobson Perovskite Solar Cells with over 15% Efficiency. *J Am Chem Soc* 142(25):11114-11122. http://10.1021/jacs.0c03363
89. Shi R, Zhang Z, Fang W-H, and Long R (2020) Charge localization control of electron–hole recombination in multilayer two-dimensional Dion–Jacobson hybrid perovskites. *Journal of Materials Chemistry A* 8(18):9168-9176. http://10.1039/d0ta01944e
90. Mao L, Guo P, Kepenekian M, Spanopoulos I, He Y, Katan C, Even J, Schaller R D, Seshadri R, Stoumpos C C, and Kanatzidis M G (2020) Organic Cation Alloying on Intralayer A and Interlayer A' sites in 2D Hybrid Dion-Jacobson Lead Bromide Perovskites (A')(A)Pb_2Br_7. *J Am Chem Soc* 142(18):8342-8351. http://10.1021/jacs.0c01625
91. Kong L, Liu G, Gong J, Mao L, Chen M, Hu Q, Lu X, Yang W, Kanatzidis M G, and Mao H K (2020) Highly tunable properties in pressure-treated two-dimensional Dion-Jacobson perovskites. *Proc Natl Acad Sci U S A* 117(28):16121-16126. http://10.1073/pnas.2003561117
92. Wang H, Chan C C S, Chu M, Xie J, Zhao S, Guo X, Miao Q, Wong K S, Yan K, and Xu J (2020) Interlayer Cross-Linked 2D Perovskite Solar Cell with Uniform Phase Distribution and Increased Exciton Coupling. *Solar RRL* 4(4). http://10.1002/solr.201900578
93. Ahmad S, Lu R, Liu Y, Liu X, Yang Q, Guo X, and Li C (2022) Cesium-doped Dion-Jacobson 2D perovskites for highly stable photovoltaics with an 18.3% efficiency. *Nano Energy* 103. http://10.1016/j.nanoen.2022.107822
94. Zhang X, Yang T, Ren X, Zhang L, Zhao K, and Liu S (2021) Film Formation Control for High Performance Dion–Jacobson 2D Perovskite Solar Cells. *Advanced Energy Materials* 11(19). http://10.1002/aenm.202002733
95. Guo W, Yang Z, Dang J, and Wang M (2021) Progress and perspective in Dion-Jacobson phase 2D layered perovskite optoelectronic applications. *Nano Energy* 86. http://10.1016/j.nanoen.2021.106129
96. Park I H, Zhang Q, Kwon K C, Zhu Z, Yu W, Leng K, Giovanni D, Choi H S, Abdelwahab I, Xu Q H, Sum T C, and Loh K P (2019) Ferroelectricity and Rashba Effect in a Two-Dimensional Dion-Jacobson Hybrid Organic-Inorganic Perovskite.

J Am Chem Soc 141(40):15972-15976. http://10.1021/jacs.9b07776
97. Zhu T, Wu H, Ji C, Zhang X, Peng Y, Yao Y, Ye H, Weng W, Lin W, and Luo J (2022) Polar Photovoltaic Effect in Chiral Alternating Cations Intercalation-Type Perovskites Driving Self-Powered Ultraviolet Circularly Polarized Light Detection. *Advanced Optical Materials* 10(15). http://10.1002/adom.202200146
98. Li P, Liang C, Liu X L, Li F, Zhang Y, Liu X T, Gu H, Hu X, Xing G, Tao X, and Song Y (2019) Low-Dimensional Perovskites with Diammonium and Monoammonium Alternant Cations for High-Performance Photovoltaics. *Adv Mater* 31(35):e1901966. http://10.1002/adma.201901966
99. Zhao Y, and Zhu K (2016) Organic-inorganic hybrid lead halide perovskites for optoelectronic and electronic applications. *Chem Soc Rev* 45(3):655-689. http://10.1039/c4cs00458b
100. Nazir G, Lee S Y, Lee J H, Rehman A, Lee J K, Seok S I, and Park S J (2022) Stabilization of Perovskite Solar Cells: Recent Developments and Future Perspectives. *Adv Mater*:e2204380. http://10.1002/adma.202204380
101. Li W, Wang Z, Deschler F, Gao S, Friend R H, and Cheetham A K (2017) Chemically diverse and multifunctional hybrid organic–inorganic perovskites. *Nature Reviews Materials* 2(3):16099. http://10.1038/natrevmats.2016.99
102. Fu Y (2022) Stabilization of Metastable Halide Perovskite Lattices in the 2D Limit. *Adv Mater* 34(9):e2108556. http://10.1002/adma.202108556
103. Correa-Baena J-P, Saliba M, Buonassisi T, Grätzel M, Abate A, Tress W, and Hagfeldt A (2017) Promises and challenges of perovskite solar cells. *Science* 358(6364):739-744. http://10.1126/science.aam6323
104. Ptak M, Maczka M, Gagor A, Sieradzki A, Stroppa A, Di Sante D, Perez-Mato J M, and Macalik L (2016) Experimental and theoretical studies of structural phase transition in a novel polar perovskite-like $[C_2H_5NH_3][Na_{0.5}Fe_{0.5}(HCOO)_3]$ formate. *Dalton Trans* 45(6):2574-2583. http://10.1039/c5dt04536c
105. Frost J M, Butler K T, Brivio F, Hendon C H, van Schilfgaarde M, and Walsh A (2014) Atomistic origins of high-performance in hybrid halide perovskite solar cells. *Nano Lett* 14(5):2584-2590. http://10.1021/nl500390f
106. Liu H, Lu Z, Zhang W, Wang J, Lu Z, Dai Q, Qi X, Shi Y, Hua Y, Chen R, Shi T, Xia H, and Wang H L (2022) Anchoring Vertical Dipole to Enable Efficient Charge Extraction for High-Performance Perovskite Solar Cells. *Adv Sci (Weinh)*:e2203640. http://10.1002/advs.202203640
107. Tian C, Zhao Y, Han X, Li B, Rui Y, Xiong H, Qiu Y, An W, Li K, Hou C, Li Y, Wang H, and Zhang Q (2023) All-in-one additive enables defect passivated, crystallization modulated and moisture resisted perovskite films toward efficient solar cells. *Chemical Engineering Journal* 452. http://10.1016/j.cej.2022.139345
108. Grancini G, and Nazeeruddin M K (2018) Dimensional tailoring of hybrid perovskites for photovoltaics. *Nature Reviews Materials* 4(1):4-22. http://10.1038/s41578-018-0065-0
109. Zhao X, Liu T, and Loo Y L (2022) Advancing 2D Perovskites for Efficient and Stable Solar Cells: Challenges and Opportunities. *Adv Mater* 34(3):e2105849. http://10.1002/adma.202105849

110. Kim B, and Seok S I (2020) Molecular aspects of organic cations affecting the humidity stability of perovskites. *Energy & Environmental Science* 13(3):805-820. http://10.1039/c9ee03473k
111. Kore B P, and Gardner J M (2020) Water-resistant 2D lead(ii) iodide perovskites: correlation between optical properties and phase transitions. *Materials Advances* 1(7):2395-2400. http://10.1039/d0ma00577k
112. Kore B P, Zhang W, Hoogendoorn B W, Safdari M, and Gardner J M (2021) Moisture tolerant solar cells by encapsulating 3D perovskite with long-chain alkylammonium cation-based 2D perovskite. *Communications Materials* 2(1). http://10.1038/s43246-021-00200-8
113. Li G, Song J, Wu J, Xu Y, Deng C, Song Z, Wang X, Du Y, Chen Q, Li R, Sun W, and Lan Z (2022) Surface defect passivation by 1,8-Naphthyridine for efficient and stable Formamidinium-based 2D/3D perovskite solar cells. *Chemical Engineering Journal* 449. http://10.1016/j.cej.2022.137806
114. Yu Y, Liu R, Liu C, Shi X L, Yu H, and Chen Z G (2022) Synergetic Regulation of Oriented Crystallization and Interfacial Passivation Enables 19.1% Efficient Wide-Bandgap Perovskite Solar Cells. *Advanced Energy Materials*. http://10.1002/aenm.202201509
115. Liu T, Guo J, Lu D, Xu Z, Fu Q, Zheng N, Xie Z, Wan X, Zhang X, Liu Y, and Chen Y (2021) Spacer Engineering Using Aromatic Formamidinium in 2D/3D Hybrid Perovskites for Highly Efficient Solar Cells. *ACS Nano* 15(4):7811-7820. http://10.1021/acsnano.1c02191
116. Uzurano G, Kuwahara N, Saito T, Fujii A, and Ozaki M (2022) Orientation Control of 2D Perovskite in 2D/3D Heterostructure by Templated Growth on 3D Perovskite. *ACS Materials Letters* 4(2):378-384. http://10.1021/acsmaterialslett.1c00709
117. Xiong M, Zou W, Fan K, Qin C, Li S, Fei L, Jiang J, Huang H, Shen L, Gao F, Jen A K Y, and Yao K (2022) Tailoring Phase Purity in the 2D/3D Perovskite Heterostructures Using Lattice Mismatch. *ACS Energy Letters* 7(1):550-559. http://10.1021/acsenergylett.1c02580
118. Jeong S, Seo S, Yang H, Park H, Shin S, Ahn H, Lee D, Park J H, Park N G, and Shin H (2021) Cyclohexylammonium-Based 2D/3D Perovskite Heterojunction with Funnel-Like Energy Band Alignment for Efficient Solar Cells (23.91%). *Advanced Energy Materials* 11(42). http://10.1002/aenm.202102236
119. Zhang Y, Chen J, Lian X, Yang W, Li J, Tian S, Wu G, and Chen H (2019) Highly efficient and thermal stable guanidinium-based two-dimensional perovskite solar cells via partial substitution with hydrophobic ammonium. *Science China Chemistry* 62(7):859-865. http://10.1007/s11426-018-9435-6
120. Ali N, Rauf S, Kong W, Ali S, Wang X, Khesro A, Yang C P, Zhu B, and Wu H (2019) An overview of the decompositions in organo-metal halide perovskites and shielding with 2-dimensional perovskites. *Renewable and Sustainable Energy Reviews* 109:160-186. http://10.1016/j.rser.2019.04.022
121. Jung E H, Jeon N J, Park E Y, Moon C S, Shin T J, Yang T Y, Noh J H, and Seo J (2019) Efficient, stable and scalable perovskite solar cells using poly(3-hexylthiophene). *Nature* 567(7749):511-515. http://10.1038/s41586-019-1036-3

122. He Q, Worku M, Xu L, Zhou C, Lin H, Robb A J, Hanson K, Xin Y, and Ma B (2020) Facile Formation of 2D-3D Heterojunctions on Perovskite Thin Film Surfaces for Efficient Solar Cells. *ACS Appl Mater Interfaces* 12(1):1159-1168. http://10.1021/acsami.9b17851
123. Quintero-Bermudez R, Gold-Parker A, Proppe A H, Munir R, Yang Z, Kelley S O, Amassian A, Toney M F, and Sargent E H (2018) Compositional and orientational control in metal halide perovskites of reduced dimensionality. *Nat Mater* 17(10):900-907. http://10.1038/s41563-018-0154-x
124. Jiang Q, Zhao Y, Zhang X, Yang X, Chen Y, Chu Z, Ye Q, Li X, Yin Z, and You J (2019) Surface passivation of perovskite film for efficient solar cells. *Nature Photonics* 13(7):460-466. http://10.1038/s41566-019-0398-2
125. Yoo J J, Wieghold S, Sponseller M C, Chua M R, Bertram S N, Hartono N T P, Tresback J S, Hansen E C, Correa-Baena J-P, Bulović V, Buonassisi T, Shin S S, and Bawendi M G (2019) An interface stabilized perovskite solar cell with high stabilized efficiency and low voltage loss. *Energy & Environmental Science* 12(7):2192-2199. http://10.1039/c9ee00751b
126. Tsai H, Nie W, Blancon J C, Stoumpos C C, Asadpour R, Harutyunyan B, Neukirch A J, Verduzco R, Crochet J J, Tretiak S, Pedesseau L, Even J, Alam M A, Gupta G, Lou J, Ajayan P M, Bedzyk M J, and Kanatzidis M G (2016) High-efficiency two-dimensional Ruddlesden-Popper perovskite solar cells. *Nature* 536(7616):312-316. http://10.1038/nature18306
127. Grancini G, Roldan-Carmona C, Zimmermann I, Mosconi E, Lee X, Martineau D, Narbey S, Oswald F, De Angelis F, Graetzel M, and Nazeeruddin M K (2017) One-Year stable perovskite solar cells by 2D/3D interface engineering. *Nat Commun* 8:15684. http://10.1038/ncomms15684
128. Yao Q, Xue Q, Li Z, Zhang K, Zhang T, Li N, Yang S, Brabec C J, Yip H L, and Cao Y (2020) Graded 2D/3D Perovskite Heterostructure for Efficient and Operationally Stable MA-Free Perovskite Solar Cells. *Adv Mater* 32(26):e2000571. http://10.1002/adma.202000571
129. Li M H, Yeh H H, Chiang Y H, Jeng U S, Su C J, Shiu H W, Hsu Y J, Kosugi N, Ohigashi T, Chen Y A, Shen P S, Chen P, and Guo T F (2018) Highly Efficient 2D/3D Hybrid Perovskite Solar Cells via Low-Pressure Vapor-Assisted Solution Process. *Adv Mater* 30(30):e1801401. http://10.1002/adma.201801401
130. He X, Wang M, Cao F, Tian W, and Li L (2022) Hydrophobic long alkyl chain organic cations induced 2D/3D heterojunction for efficient and stable perovskite solar cells. *Journal of Materials Science & Technology* 124:243-251. http://10.1016/j.jmst.2022.01.031
131. Fan W, Shen Y, Deng K, Chen Q, and Bai Y (2021) A tailored spacer molecule in 2D/3D heterojunction for ultralow-voltage-loss and stable perovskite solar cells. *Journal of Materials Chemistry A* 9(47):26829-26838. http://10.1039/d1ta08984f
132. Jang Y-W, Lee S, Yeom K M, Jeong K, Choi K, Choi M, and Noh J H (2021) Intact 2D/3D halide junction perovskite solar cells via solid-phase in-plane growth. *Nature Energy* 6(1):63-71. http://10.1038/s41560-020-00749-7
133. Chen C, Liang J, Zhang J, Liu X, Yin X, Cui H, Wang H, Wang C, Li Z, Gong

J, Lin Q, Ke W, Tao C, Da B, Ding Z, Xiao X, and Fang G (2021) Interfacial engineering of a thiophene-based 2D/3D perovskite heterojunction for efficient and stable inverted wide-bandgap perovskite solar cells. *Nano Energy* 90. http://10.1016/j.nanoen.2021.106608

134. Beal R E, Hagström N Z, Barrier J, Gold-Parker A, Prasanna R, Bush K A, Passarello D, Schelhas L T, Brüning K, Tassone C J, Steinrück H-G, McGehee M D, Toney M F, and Nogueira A F (2020) Structural Origins of Light-Induced Phase Segregation in Organic-Inorganic Halide Perovskite Photovoltaic Materials. *Matter* 2(1):207-219. http://10.1016/j.matt.2019.11.001

135. Chen B, Rudd P N, Yang S, Yuan Y, and Huang J (2019) Imperfections and their passivation in halide perovskite solar cells. *Chemical Society Reviews* 48(14):3842-3867. http://10.1039/C8CS00853A

136. Liu B, Hu J, He D, Bai L, Zhou Q, Wang W, Xu C, Song Q, Lee D, Zhao P, Hao F, Niu X, Zang Z, and Chen J (2022) Simultaneous Passivation of Bulk and Interface Defects with Gradient 2D/3D Heterojunction Engineering for Efficient and Stable Perovskite Solar Cells. *ACS Appl Mater Interfaces* 14(18):21079-21088. http://10.1021/acsami.2c04374

137. He M, Liang J, Zhang Z, Qiu Y, Deng Z, Xu H, Wang J, Yang Y, Chen Z, and Chen C-C (2020) Compositional optimization of a 2D–3D heterojunction interface for 22.6% efficient and stable planar perovskite solar cells. *Journal of Materials Chemistry A* 8(48):25831-25841. http://10.1039/d0ta09209f

138. Kim H, Lee S U, Lee D Y, Paik M J, Na H, Lee J, and Seok S I (2019) Optimal Interfacial Engineering with Different Length of Alkylammonium Halide for Efficient and Stable Perovskite Solar Cells. *Advanced Energy Materials* 9(47). http://10.1002/aenm.201902740

139. Chen P, Bai Y, Wang S, Lyu M, Yun J H, and Wang L (2018) In Situ Growth of 2D Perovskite Capping Layer for Stable and Efficient Perovskite Solar Cells. *Advanced Functional Materials* 28(17). http://10.1002/adfm.201706923

140. Chen S, Dai X, Xu S, Jiao H, Zhao L, and Huang J (2021) Stabilizing perovskite-substrate interfaces for high-performance perovskite modules. *Science* 373(6557):902-907. http://10.1126/science.abi6323

141. Chen B, Chen H, Hou Y, Xu J, Teale S, Bertens K, Chen H, Proppe A, Zhou Q, Yu D, Xu K, Vafaie M, Liu Y, Dong Y, Jung E H, Zheng C, Zhu T, Ning Z, and Sargent E H (2021) Passivation of the Buried Interface via Preferential Crystallization of 2D Perovskite on Metal Oxide Transport Layers. *Adv Mater* 33(41):e2103394. http://10.1002/adma.202103394

142. Xia J, Liang C, Mei S, Gu H, He B, Zhang Z, Liu T, Wang K, Wang S, Chen S, Cai Y, and Xing G (2021) Deep surface passivation for efficient and hydrophobic perovskite solar cells. *Journal of Materials Chemistry A* 9(5):2919-2927. http://10.1039/d0ta10535j

143. Malouangou M D, Yang Y, Zhang Y, Bai L, Matondo J T, Mbumba M, Akram M W, and Guli M (2022) Facilitate hole transport with thin 2D perovskite capping layer to passivate interface defects of 3D perovskite solar cells using PEABr. *Materials Research Bulletin* 150. http://10.1016/j.materresbull.2022.111793

144. Yukta, Parikh N, Chavan R D, Yadav P, Nazeeruddin M K, and Satapathi S (2022) Highly Efficient and Stable 2D Dion Jacobson/3D Perovskite Heterojunction Solar Cells. *ACS Appl Mater Interfaces* 14(26):29744-29753. http://10.1021/acsami.2c04455
145. Zheng H, Dong X, Wu W, Liu G, and Pan X (2022) Multifunctional Heterocyclic-Based Spacer Cation for Efficient and Stable 2D/3D Perovskite Solar Cells. *ACS Appl Mater Interfaces* 14(7):9183-9191. http://10.1021/acsami.1c23991
146. Li Y, Zhang J, Xiang J, Hu H, Zhong H, and Shi Y (2022) A Novel 4,4'-Bipiperidine-Based Organic Salt for Efficient and Stable 2D-3D Perovskite Solar Cells. *ACS Appl Mater Interfaces* 14(19):22324-22331. http://10.1021/acsami.1c23115
147. Xu J, Cui J, Yang S, Liu Z, Guo X, Che Y, Xu D, Zhao W, Yuan N, Ding J, and Liu S (2022) Stable High-Efficiency $CsPbI_2Br$ Solar Cells by Designed Passivation Using Multifunctional 2D Perovskite. *Advanced Functional Materials*. http://10.1002/adfm.202202829
148. Zhang X, Zhou W, Chen X, Chen Y, Li X, Wang M, Zhou Y, Yan H, Zheng Z, and Zhang Y (2022) Dual Optimization of Bulk and Surface via Guanidine Halide for Efficient and Stable 2D/3D Hybrid Perovskite Solar Cells. *Advanced Energy Materials* 12(26). http://10.1002/aenm.202201105
149. Zhou T, Xu Z, Wang R, Dong X, Fu Q, and Liu Y (2022) Crystal Growth Regulation of 2D/3D Perovskite Films for Solar Cells with Both High Efficiency and Stability. *Adv Mater* 34(17):e2200705. http://10.1002/adma.202200705
150. Azmi R, Ugur E, Seitkhan A, Aljamaan F, Subbiah A S, Liu J, Harrison G T, Nugraha M I, Eswaran M K, Babics M, Chen Y, Xu F, Allen T G, Rehman A u, Wang C-L, Anthopoulos T D, Schwingenschlögl U, De Bastiani M, Aydin E, and De Wolf S (2022) Damp heat–stable perovskite solar cells with tailored-dimensionality 2D/3D heterojunctions. *Science* 376(6588):73-77. http://10.1126/science.abm5784
151. Jin M, Li H, Lou Q, Du Q, Huang Q, Shen Z, Li F, and Chen C (2022) Toward high-efficiency stable 2D/3D perovskite solar cells by incorporating multifunctional CNT:TiO_2 additives into 3D perovskite layer. *EcoMat* 4(2). http://10.1002/eom2.12166
152. Deng C, Wu J, Du Y, Chen Q, Song Z, Li G, Wang X, Lin J, Sun W, Huang M, Huang Y, Gao P, and Lan Z (2021) Surface Reconstruction and In Situ Formation of 2D Layer for Efficient and Stable 2D/3D Perovskite Solar Cells. *Small Methods* 5(12):e2101000. http://10.1002/smtd.202101000
153. Ye X, Cai H, Sun Q, Xu T, Ni J, Li J, and Zhang J (2022) Organic spacer engineering in 2D/3D hybrid perovskites for efficient and stable solar cells. *New Journal of Chemistry* 46(6):2837-2845. http://10.1039/d1nj05232b
154. Yang S, Dai J, Yu Z, Shao Y, Zhou Y, Xiao X, Zeng X C, and Huang J (2019) Tailoring Passivation Molecular Structures for Extremely Small Open-Circuit Voltage Loss in Perovskite Solar Cells. *J Am Chem Soc* 141(14):5781-5787. http://10.1021/jacs.8b13091
155. Lin C T, Lee J, Kim J, Macdonald T J, Ngiam J, Xu B, Daboczi M, Xu W, Pont

S, Park B, Kang H, Kim J S, Payne D J, Lee K, Durrant J R, and McLachlan M A (2019) Origin of Open-Circuit Voltage Enhancements in Planar Perovskite Solar Cells Induced by Addition of Bulky Organic Cations. *Advanced Functional Materials* 30(7). http://10.1002/adfm.201906763

156. Zhou J, Li M, Wang S, Tan L, Liu Y, Jiang C, Zhao X, Ding L, and Yi C (2022) 2-CF_3-PEAI to eliminate Pb^0 traps and form a 2D perovskite layer to enhance the performance and stability of perovskite solar cells. *Nano Energy* 95. http://10.1016/j.nanoen.2022.107036

157. Milot R L, Sutton R J, Eperon G E, Haghighirad A A, Martinez Hardigree J, Miranda L, Snaith H J, Johnston M B, and Herz L M (2016) Charge-Carrier Dynamics in 2D Hybrid Metal-Halide Perovskites. *Nano Lett* 16(11):7001-7007. http://10.1021/acs.nanolett.6b03114

158. Stoumpos C C, Cao D H, Clark D J, Young J, Rondinelli J M, Jang J I, Hupp J T, and Kanatzidis M G (2016) Ruddlesden–Popper Hybrid Lead Iodide Perovskite 2D Homologous Semiconductors. *Chemistry of Materials* 28(8):2852-2867. http://10.1021/acs.chemmater.6b00847

159. Chen R, Shen L, Zheng L, Zhu T, Liu Y, Liu L, Zheng J, and Gong X (2021) Two-/Three-Dimensional Perovskite Bilayer Thin Films Post-Treated with Solvent Vapor for High-Performance Perovskite Photovoltaics. *ACS Appl Mater Interfaces* 13(41):49104-49113. http://10.1021/acsami.1c15735

160. Buizza L R V, Crothers T W, Wang Z, Patel J B, Milot R L, Snaith H J, Johnston M B, and Herz L M (2019) Charge-Carrier Dynamics, Mobilities, and Diffusion Lengths of 2D–3D Hybrid Butylammonium–Cesium–Formamidinium Lead Halide Perovskites. *Advanced Functional Materials* 29(35). http://10.1002/adfm.201902656

161. Liu Y, Akin S, Pan L, Uchida R, Arora N, Milić J V, Hinderhofer A, Schreiber F, Uhl A R, Zakeeruddin S M, Hagfeldt A, Dar M I, and Grätzel M Ultrahydrophobic 3D/2D fluoroarene bilayer-based water-resistant perovskite solar cells with efficiencies exceeding 22%. *Science Advances* 5(6):eaaw2543. http://10.1126/sciadv.aaw2543

162. Li Y, Wu J, Zhang Y, Zhang L, Zhou X, Hu B, Jiang Z, Zeng J, Wang D, Liu Y, Chen S, Liu Z, Liu C, Wang X, and Xu B (2022) Whether organic spacer cations induced 2D/3D or quasi-2D/3D mixed dimensional perovskites? *Chemical Engineering Journal* 450. http://10.1016/j.cej.2022.137887

163. Pareja-Rivera C, Morán-Muñoz J A, Gómora-Figueroa A P, Jancik V, Vargas B, Rodríguez-Hernández J, and Solis-Ibarra D (2022) Optimizing Broadband Emission in 2D Halide Perovskites. *Chemistry of Materials*. http://10.1021/acs.chemmater.2c00937

164. Chen H, Lin J, Kang J, Kong Q, Lu D, Kang J, Lai M, Quan L N, Lin Z, Jin J, Wang L-w, Toney M F, and Yang P Structural and spectral dynamics of single-crystalline Ruddlesden-Popper phase halide perovskite blue light-emitting diodes. *Science Advances* 6(4):eaay4045. http://10.1126/sciadv.aay4045

165. Jana M K, Song R, Xie Y, Zhao R, Sercel P C, Blum V, and Mitzi D B (2021) Structural descriptor for enhanced spin-splitting in 2D hybrid perovskites. *Nat*

Commun 12(1):4982. http://10.1038/s41467-021-25149-7
166. Chen Z, Guo Y, Wertz E, and Shi J (2019) Merits and Challenges of Ruddlesden-Popper Soft Halide Perovskites in Electro-Optics and Optoelectronics. *Adv Mater* 31(1):e1803514. http://10.1002/adma.201803514
167. Dhanabalan B, Leng Y C, Biffi G, Lin M L, Tan P H, Infante I, Manna L, Arciniegas M P, and Krahne R (2020) Directional Anisotropy of the Vibrational Modes in 2D-Layered Perovskites. *ACS Nano* 14(4):4689-4697. http://10.1021/acsnano.0c00435
168. Torma A J, Li W, Zhang H, Tu Q, Klepov V V, Brennan M C, McCleese C L, Krzyaniak M D, Wasielewski M R, Katan C, Even J, Holt M V, Grusenmeyer T A, Jiang J, Pachter R, Kanatzidis M G, Blancon J C, and Mohite A D (2021) Interstitial Nature of $Mn^{(2+)}$ Doping in 2D Perovskites. *ACS Nano* 15(12):20550-20561. http://10.1021/acsnano.1c09142
169. Pham M T, Amerling E, Ngo T A, Luong H M, Hansen K, Pham H T, Vu T N, Tran H, Whittaker-Brooks L, and Nguyen T D (2021) Strong Rashba-Dresselhaus Effect in Nonchiral 2D Ruddlesden-Popper Perovskites. *Advanced Optical Materials* 10(1). http://10.1002/adom.202101232
170. Yan L, Jana M K, Sercel P C, Mitzi D B, and You W (2021) Alkyl-Aryl Cation Mixing in Chiral 2D Perovskites. *J Am Chem Soc* 143(43):18114-18120. http://10.1021/jacs.1c06841
171. Kim D, Dryzhakov B, Liu Y, Ovchinnikova O S, Hu B, Kalinin S V, and Ahmadi M (2021) Ferroelectric and Charge Transport Properties in Strain-Engineered Two-Dimensional Lead Iodide Perovskites. *Chemistry of Materials* 33(11):4077-4088. http://10.1021/acs.chemmater.1c00679
172. Kumar A, Solanki A, Manjappa M, Ramesh S, Srivastava Y K, Agarwal P, Sum T C, and Singh R Excitons in 2D perovskites for ultrafast terahertz photonic devices. *Science Advances* 6(8):eaax8821. http://10.1126/sciadv.aax8821
173. Li N, Apergi S, Chan C C S, Jia Y, Xie F, Liang Q, Li G, Wong K S, Brocks G, Tao S, and Zhao N (2022) Diammonium-Mediated Perovskite Film Formation for High-Luminescence Red Perovskite Light-Emitting Diodes. *Adv Mater* 34(30):e2202042. http://10.1002/adma.202202042
174. Tao W, Zhang Y, and Zhu H (2022) Dynamic Exciton Polaron in Two-Dimensional Lead Halide Perovskites and Implications for Optoelectronic Applications. *Acc Chem Res* 55(3):345-353. http://10.1021/acs.accounts.1c00626